NASA CONTRACTOR REPORT

NASA CR-2354

NASA CR-2354

THEORETICAL STUDIES OF TONE NOISE FROM A FAN ROTOR

by G. V. R. Rao, W. T. Chu, and R. V. Digumarthi

Prepared by
RAO AND ASSOCIATES, INC.
Sherman Oaks, Calif.
for Ames Research Center

NATIONAL AERONAUTICS AND SPACE ADMINISTRATION • WASHINGTON, D. C. • NOVEMBER 1973

1. Report No.	2. Government Accession No.	3. Recipient's Catalog No.
NASA CR-2354		

4. Title and Subtitle	5. Report Date
"Theoretical Studies of Tone Noise From a Fan Rotor"	November 1973
	6. Performing Organization Code

7. Author(s)	8. Performing Organization Report No.
G.V.R. Rao, W.T. Chu, and R.V. Digumarthi	
	10. Work Unit No.

9. Performing Organization Name and Address	11. Contract or Grant No.
Rao and Associates, Inc. 14827 Ventura Boulevard Sherman Oaks, California	NAS 2-6401
	13. Type of Report and Period Covered
12. Sponsoring Agency Name and Address	Final Report
National Aeronautics & Space Administration Washington, D.C. 20546	14. Sponsoring Agency Code

15. Supplementary Notes

16. Abstract

An analytical study was made of some possible rotor alone noise sources of dipole, quadrapole and monopole characters which generate discrete tone noise. Particular emphasis is given to the tone noise caused by fan inlet flow distortion and turbulence. Analytical models are developed to allow prediction of absolute levels. Experimental data measured on a small scale fan is presented which indicates inlet turbulence interaction with a fan rotor can be a source of tone noise. Predicted and measured tone noise for the small scale rotor are shown to be in reasonable agreement.

17. Key Words (Suggested by Author(s))	18. Distribution Statement
rotor alone noise sources	UNCLASSIFIED - UNLIMITED

19. Security Classif. (of this report)	20. Security Classif. (of this page)	21. No. of Pages	22. Price*
UNCLASSIFIED	UNCLASSIFIED	78	Domestic, $3.75 Foreign, $6.25

* For sale by the National Technical Information Service, Springfield, Virginia 22151

THEORETICAL STUDIES OF TONE NOISE FROM A FAN ROTOR

By G.V.R. Rao, W.T. Chu, and R.V. Digumarthi
Rao and Associates, Inc.

SUMMARY

Noise sources in a fan rotor due to inflow distortion and turbulence are examined. Analytical studies show that high levels of tone noise at blade passing frequency and its higher harmonics can result from relatively small distortions of the inflow to the rotor. It is shown that these discrete tones can also originate from blade loading fluctuations caused by inflow turbulence, provided the longitudinal velocity correlation length scale is sufficiently large. Computations carried out on a small scale subsonic rotor indicate that acoustic radiation from blade thickness effect and fluctuating Reynolds stresses is small compared to that from blade loading. Theoretical predictions of on-axis noise are in reasonable agreement with acoustic measurements taken on a small scale rotor.

TABLE OF CONTENTS

LIST OF SYMBOLS

B	number of blades
C_L	blade section lift coefficient
K	nondimensionalized wave number
L	lift on blade per unit span
M	Mach number
N	rotor rps
R	distance of field point from the rotor center
S	distance of the field point from source
U	inflow velocity
U_a	mean axial velocity through the rotor
U_p	velocity fluctuations due to potential flow around blades
V_r	mean relative velocity at the rotor
V_t	blade tangential velocity
a_o	ambient speed of sound
b	blade section thickness
c	blade chord
d	blade spacing
ℓ	longitudinal velocity correlation length
n	harmonic index
p	far field acoustic pressure
r	radius
u	turbulent velocity

Φ	power spectral density
Ψ	azimuthal angle
Ω	rotor circular frequency
ζ	distance along the blade chord from midchord, positive toward trailing edge
θ	angle from reference meridional plane, positive in the direction of rotor rotation
λ	blade stagger angle
ν	circular frequency of far field acoustic pressure
ρ_o	ambient air density
σ	solidity of rotor
ω	circular frequency of velocity fluctuations

Subscripts

e	at effective radius
h	at hub
n	nth harmonic component
r	component along mean relative velocity
t	at tip
ι	component normal to mean relative velocity
1,2,3	components in axial, radial and tangential directions respectively
g,h,m	integer indicies
j	pertaining to the jth blade counted in the direction of rotation from reference meridional plane

Superscripts

$\hat{}$	amplitude
~	root mean square value
—	temporal mean
d	due to dipole radiation
s	due to monopole radiation
q	due to quadrupole radiation

Special symbols

δL	elemental force on area $rd\theta dr$
δp	far field acoustic pressure due to force δL, volume source δq , or quadrupole source defined by Eq. (3.17).
δq	elemental volume source contained in volume $(d\zeta\, dr\ r\, d\theta)$.

1.0 INTRODUCTION

The various mechanisms by which noise is generated in a lift fan have been the subject of an analytical study during the past two years, at Rao and Associates, Inc., under a contract with National Aeronautics and Space Administration. Lift fans operate essentially on the same principles as a single stage compressor or a turbo-fan, and the acoustic studies on such machines, carried out by several investigators over the past decade, guided us in our investigations. Noise measurements on a small scale fan[1] and on the various OGV configurations of the 36 inch diameter GE LF336 lift fan[2] indicated high level discrete tones, contrary to theoretical predictions of blade-vane interaction effects. Consequently, the noise sources associated with the rotor itself are investigated further and some preliminary results were presented in our interim report[3] on the contract.

The noise sources, whether they be from forces or flow interactions can be classified into two general catagories: ordered and random. In the first catagory, the sources at any one point in the flow region have a deterministic relation with those at any other point. When the sources are random, as in the second catagory, we can only mention the spectral distribution of the source strength and correlation over limited separation distances. Ordered sources, except in a specific type of inflow distortion, radiate zero tone-noise to

points on rotor axis, contrary to the high levels observed in test data, and therefore emphasis is given in this report to random noise sources and radiation to on-axis points.

Since the noise generated in a fan is governed by the velocities occurring through the fan, our report begins with a description of flow field as given in section 2. The consequences of the flow, such as forces on blades, effect of their thickness and the occurrence of fluctuating Reynolds stresses are also discussed in this section. The presence of a rotating blade, i.e. its loading and thickness, are replaced by suitably phased elemental dipoles and monopoles around the rotor circumference, and sound radiation from all such sources in the fan annulus is examined in the following two sections. The influence of inflow distortion is discussed in section 3 and the effect of turbulence in the inflow to the rotor is treated in section 4. Acoustic radiation from fluctuating Reynolds stresses is evaluated in these sections using the space-time correlation functions of the velocity fluctuations. Our primary effort is on estimation of noise sources occurring in a fan-rotor, and the effect of duct cut-off has been ignored in the preliminary noise calculations carried out on the small scale fan and presented here. It is observed that the random loading on the rotor blades caused by inflow turbulence, with sufficiently large length scale, can give rise to discrete tone noise at blade passing frequency and its higher harmonics. The configuration of the small

scale rotor used in our acoustic computations is described in reference 1, and the pertinent design parameters are given in Fig. 1.1.

Inflow turbulence and on-axis noise measurements obtained by NASA Ames Research Center on the small scale rotor are presented in section 5. Acoustic computations, at the flow parameters corresponding to the test conditions, show reasonable agreement with measured noise levels. Conclusions and recommendations for future investigations are given in the final section of this report.

The theoretical investigations and acoustic computations were carried out at Rao and Associates, Inc., for NASA Ames Research Center under contract NAS2-6401. The helpful suggestions by Mr. B.K. Hodder and Mr. D.H. Hickey, the technical managers on this contract, are greatly appreciated.

2.0 NOISE SOURCES IN A ROTOR

A comprehensive theory of generation and propagation of aerodynamic sound is given by Lighthill[4] in his 1961 Bakerian Lecture. Following his approach, the rotor noise problem can be investigated by considering the role of the following:

(a) Aerodynamic forces on the blades giving rise to acoustic dipoles.

(b) Effect of blade thickness giving rise to acoustic monopoles.

(c) Fluctuating Reynolds stresses, and the resulting quadrupoles.

The monopole and dipole sources are located at the blades, whereas the quadrupole sources are present in the entire flow region exterior to the blades. All the above noise sources are directly related to the velocities occurring in the region of the rotor and hence a description of the flow field is given in this section, followed by a general discussion of the sources and their locations. The coordinate system employed in describing the flow field and blade locations is shown in Fig. 2.1.

2.1 Description of Flow Field

The velocity field in a fan, including the effect of moving rotor blades and stationary vanes or struts has been described in detail in reference 3. Since the present investigation is limited to noise from the rotor itself, we shall limit our attention only to the effect of rotor blades. The

flow conditions within the wake of each blade have considerable random components, unrelated to the conditions occurring in the wakes of the neighboring blades, as pointed out in reference 5, and such velocity fluctuations by themselves do not contribute to discrete tone noise. Consequently, we shall exclude the region downstream of the rotor and describe the velocity vector in the flow region as

$$\vec{V} = \vec{U} + \vec{U}_p + \vec{u} \tag{2.1}$$

The inflow to the fan, denoted by $\vec{U}$, may be both unsteady and nonuniform. The velocity resulting from the potential flow around the rotating blades is represented by $\vec{U}_p$. The last term $\vec{u}$ denotes the turbulent fluctuations of velocity in the inflow. We note that each term, except $\vec{u}$, in the above equation is well correlated, i.e. the value at any one point is definable in terms of its value at any other point. On the other hand, the turbulent fluctuations $\vec{u}$ may have correlation only in a small region.

In the following discussion, we will be describing the velocities in terms of their components in the axial, radial and tangential directions indicated in Fig. 2.1, by using subscripts 1, 2, and 3 respectively. Subscripts r and ı will be used to denote respectively the components along and normal to the mean relative velocity met by the rotor blade.

2.1.1 Inflow to the fan

Due to disturbances upstream of a fan engine, the inflow to the rotor can exhibit spatial nonuniformity as well as fluctuations of such distorted flow. At any given location in the fan annulus, the inflow velocity $\vec{U}$ can be described by its components in the axial, radial and tangential directions. However, the fluctuations of lift loading on the blades is primarily dependent upon the component normal to the relative velocity. Denoting this component of the inflow by $U_\perp$, we can express its periodic fluctuations as

$$U_\perp(r,\theta,t) = \sum_h \hat{U}_{h,\perp}(r,\theta)\cdot e^{-i(\omega_h t+\phi_h)} \qquad (2.2)$$

We note that the left hand side is a real function in the above representation. Here and in the rest of this report, when no limits are shown, the summation is over all integer values from $-\infty$ to $+\infty$ including zero. The steady state value of $U_\perp$ is the term for $h = 0$. The variation $U_{h,\perp}$ in the θ direction can also be represented by a similar complex Fourier series to allow the following description

$$\begin{aligned} U_\perp(r,\theta,t) &= \sum_g \sum_h \hat{U}_{gh,\perp}\cdot e^{i(g\theta+\phi_g)}\cdot e^{-i(\omega_h t+\phi_h)} \\ &= \sum_g \sum_h \hat{U}_{gh,\perp}\cdot e^{i(g\theta-\omega_h t+\phi_{gh})} \end{aligned} \qquad (2.3)$$

Above description of velocity allows different functions of t to represent the temporal fluctuations at different positions

in the annulus. However, the frequency ω_h of the ghth component is independent of the coordinates r,θ. This requirement is consistent with ignoring the random disturbance in the present treatment. The amplitudes $\hat{U}_{gh,1}$ and phase angles ϕ_{gh} can be determined from Fourier analysis of flow field survey at the fan inlet. The lowest frequency ω_h employed in the above equation corresponds to the longest period one finds from the fluctuations at various locations in the annulus. We note that Eq. (2.3) represents uniform axial inflow conditions when ω_h and g are both zero.

In considering the effect of blade thickness, by suitable source-sink distribution, we require the knowledge of the velocity component along the blade chord, which can be approximated by the component U_r, taken along the mean relative velocity direction. Similar to Eq. (2.3) we can deduce the expression

$$U_r(r,\theta,t) = \sum_g \sum_h \hat{U}_{gh,r} \cdot e^{i(g\theta - \omega_h t + \phi_{gh})} \qquad (2.4)$$

2.1.2 Potential flow around blades

Let us consider an elemental annulus $2\pi r dr$ of the fan containing B number of equally spaced identical blades. The potential flow around these blades can be obtained in terms of two-dimensional flow past a cascade of infinite number of airfoils. Each airfoil in the cascade can be replaced by suitable distribution of vortices, sources and sinks to evaluate the

flow field due to lift on the blades and the effect of their thickness. Such analysis was presented in reference 3, and it was found that a simplified description of the flow field upstream of the leading edges is possible. The perturbations from the mean flow are relatively small in the region downstream of the rotor leading edge and hence will be ignored in the noise calculation presented in this report.

Based on reference 3, we can write the following expression for the periodic fluctuations of the axial component of the rotor-induced velocity in the region upstream of rotor leading edge.

$$U_{p_1} = \sum_n U_{p_1,n} \tag{2.5}$$

where $U_{p_1,n} = \hat{U}_{p_1,n} \cdot e^{-|2n\pi\eta_1/d|} \cdot \exp\{i\phi_{p_1,n} + inB(\theta - \Omega t)\}$

$\hat{U}_{p_1,n}, \phi_{p_1,n}$ = the amplitude and phase angle respectively of the component at blade leading edge

η_1 = axial distance upstream from rotor leading edge

and d = blade spacing.

The amplitude $\hat{U}_{p_1,n}$ and the phase angle $\phi_{p_1,n}$ depend upon the blade loading, rotor geometry, and blade thickness distribution as discussed in reference 3.

The above simple representation for $U_{p_1,n}$ is possible upstream of rotor leading edge, since phase angle $\phi_{p_1,n}$ does not depend upon η_1 in this region. Computations at pitch radius, on the small scale fan, for the corresponding tangential component indicate

$$\hat{U}_{p_3,n} \simeq \hat{U}_{p_1,n}$$

and $$\phi_{p_3,n} = \frac{\pi}{2} + \phi_{p_1,n}$$

Consequently, we can write

$$U_{p_3,n} \simeq U_{p_1,n} \cdot e^{i\pi/2} \tag{2.6}$$

The radial components of $\vec{U}_p$ will be ignored, since the potential flow field past the rotor blades is evaluated under two-dimensional flow assumptions.

2.1.3 Inflow turbulence

The velocity perturbations discussed in preceeding subsections are well-ordered in the sense that the velocity at one point of the flow region has a definite space-time relation with the velocity at any other point of the flow region. On the other hand, the random velocity fluctuations present in the flow entering the fan can be referred to only in terms of statistical quantities such as mean square values, probability density functions, correlation functions and power spectral density functions. In the study of fan noise problems, another important quantity is the correlation length ℓ, which is defined as the area under the non-dimensional correlation function and thus represents some average size of the eddy within which two points in the flow field will have velocity fluctuations that can be considered as coherent or related.

The spectral distribution and the correlation length are not independent of each other. This is obvious for the

reason that if low frequency fluctuations are dominant, the extent to which two points in the flow field are related will be larger. The way they are related depends on the particular model chosen to describe the turbulent field, as discussed in reference 3.

Let us assume that the turbulent fluctuations in the inflow are homogeneous, isotropic and are characterized by a longitudinal velocity correlation function of the type $\exp(-|\xi|/\ell)$, where ξ is the separation distance. Choosing "frozen-convected turbulence" hypothesis, the spectra of the components u_1 and u_2 can be related to length scale ℓ and the convection velocity. From geometrical relation one can derive the spectra for u_r and $u_\perp$, as functions of spectral intensities of u_1 and u_2 and the blade stagger angle λ. In our present investigations, we can use the mean axial inflow velocity U_a as a close approximation to the convection velocity. Furthermore, the blade stagger angle being close to $\pi/2$ in general, we shall assume that $u_\perp \simeq u_1$ and $u_r \simeq u_3$, in describing the spectral intensities of $u_\perp$ and u_r. Consequently we used

$$\Phi_{u_\perp}(\omega) = \overline{u^2}\,\frac{\ell}{\pi U_a}\{1 + (\ell\omega/U_a)^2\}^{-1} \tag{2.7}$$

and

$$\Phi_{u_r}(\omega) = \overline{u^2}\,\frac{\ell}{2\pi U_a}\{1+3(\ell\omega/U_a)^2\}\{1 + (\ell\omega/U_a)^2\}^{-2} \tag{2.8}$$

in investigating the blade loading and thickness effects caused by inflow turbulence.

For the quadrupole calculations, as carried out in subsection 4.3, the space-time correlation function of u_1 is required. Without assuming isotropy, the space-time correlation function of u_1 for "frozen-pattern" convected with velocity U_a can be written as

$$R_{u_1}(\underset{\sim}{\xi},\tau) = \overline{u^2}\cdot\exp\left\{-\left|\frac{\xi_1 - U_a\tau}{\ell_1}\right| - \left|\frac{\xi_2}{\ell_2}\right| - \left|\frac{\xi_3}{\ell_3}\right|\right\} \tag{2.9}$$

where the subscripts on ℓ and ξ denote the length scales and separation distances in the respective directions. If one is interested in that part of the noise generated by the true temporal fluctuation of the turbulent field, an additional time function has to be incorporated as discussed in reference 3.

2.2 Rotor Blade Loading

Each blade element, as it travels around the circumference with a tangential velocity V_t, experiences periodic and random fluctuations in loading caused by the inflow distortions and turbulence discussed in the preceeding subsection. Typical of the airfoil profiles employed for the blades, the drag can be ignored in comparison to the lift force. Let us consider a blade element of span dr, at radius r, and experiencing a lift force Ldr, where

$$L = \frac{1}{2}\rho_0 V_r^2 C_L c \tag{2.10}$$

The lift L per unit span of the blade depends upon the relative velocity V_r, chord c, and lift coefficient C_L.

Let us assume that all the B number of blade elements are equally spaced around the circumference $2\pi r$ and have the same cross-section and stagger angle. Let subscript j identify the jth blade, as j takes on integer values increasing in the direction of rotor rotation from 1 to B. The coordinate system employed in our analysis and the location of the jth blade are typically sketched in Fig. 2.1. For the sake of convenience, the reference meridional plane $\theta = 0$ is chosen so as to contain the point, at which the far field sound pressure is evaluated in later sections. Even though all the blade elements are identical, they may not simultaneously experience the same lift force as discussed in later sections 3 and 4. To relate the point of application of load on each blade element to its position in the annulus, we assumed that the locus of mid-chord locations along the blade span is a radial line. Since the center of gravity of a blade section is not too far from its mid-chord location, such an assumption is a reasonable approximation.

The force on the jth blade can be evaluated according to Eq. (2.10) with the appropriate values of V_r and C_L as experienced by the jth blade. Considering the force L_j as concentrated at a point on the jth blade its coordinates can be derived from Fig. 2.1 as

$$x_j = -\zeta' \cos\lambda$$

$$r_j = r$$

and

$$\theta_j = \theta_1 + (j-1)\frac{2\pi}{B} - \frac{\zeta' \sin\lambda}{r} \qquad (2.11)$$

where λ = blade stagger angle,

ζ' = center of pressure measured from midchord along the chord, positive towards the trailing edge,

and θ_1 = location of midchord of "first" blade at time t.

Furthermore, if the blade with its midchord point crossing the meridional plane $\theta = 0$ at time $t = 0$ is denoted as the "first" blade, we can write

$$\theta_j = \Omega t + (j - 1)\frac{2\pi}{B} - \frac{\zeta' \sin\lambda}{r} \qquad (2.12)$$

where Ω = rotor circular frequency.

The dependence of blade loading on the inflow conditions and the resulting sound radiation is discussed in sections 3 and 4 of this report.

2.3 Volume Sources Due to Blade Thickness

The motion of the rotor blade, due to its thickness, causes air to be pushed out and drawn back respectively near the leading and trailing edge regions. Velocity perturbations normal to the rotor disc, caused by the finite thickness of blades rotating in uniform steady flow, were considered by Deming[6] to evaluate the resulting acoustic radiation. In the following, we shall consider the general case of the blades immersed in non-uniform unsteady flow and derive expressions for the fluctuating volume sources due to the effect of blade thickness. Similar to the discussion presented in the previous subsection 2.2, let us consider an element of span dr at radius r on the jth blade. The two-dimensional

flow past the blade profile can be approximated by the following distribution of source-sink strength along the chord.

$$\mathcal{A}_{\zeta j} = V_r \cdot \frac{db}{d\zeta} \tag{2.13}$$

where ζ = distance measured from midchord, along the chord, positive towards trailing edge,

V_r = relative velocity, considered parallel to blade chord,

and b = blade thickness.

The subscript ζj on the left hand side of above equation denotes the function as dependent on ζ measured on the jth blade.

Taking into account the span dr, the jth blade element can be considered as volume sources

$$q_{\zeta j} = V_r \cdot \frac{db}{d\zeta} \, d\zeta \, dr \tag{2.14}$$

located at every point $-c/2 \leq \zeta \leq c/2$ over the chord of this jth blade. The coordinates of this point ζ along the chord of the jth blade element can be written, similar to Eq. (2.11), as

$$x_{\zeta j} = -\zeta \cos\lambda$$

$$r_{\zeta j} = r$$

and

$$\theta_{\zeta j} = \Omega t + (j-1)2\pi/B - (\zeta \sin\lambda)/r \tag{2.15}$$

Sound radiation from the volume sources described above is investigated in sections 3 and 4 of this report.

2.4 "Fluctuating Reynolds Stresses" in the Flow Region

The manner in which fluctuating flows can generate noise as quadrupoles sources was originally formulated by Lighthill[7] For subsonic flow, the dominant source term is the "fluctuating Reynolds stresses"

$$T_{ij} = \rho_o V_i V_j \tag{2.16}$$

where the subscripts i,j indicate the components in the three dimensional cartesian coordinate directions 1, 2, and 3. To obtain the fluctuating Reynolds stresses T_{ij} in the flow region through the rotor, we substitute the instantaneous velocity vector $\vec{V}$ as defined by Eq. (2.1). The resulting acoustic radiation is discussed in the appendix, and application to rotor noise under various flow conditions is presented in the following sections 3 and 4.

3.0 ROTOR NOISE GENERATED BY INFLOW DISTORTIONS

A general description of inflow distortion is given in subsection 2.1.1 in terms of its ghth components. Without the knowledge of amplitude, frequency and phase angle of each ghth component, it is difficult to evaluate the noise generated by inflow distortion. However, we can proceed to examine the sound radiation resulting from blade loading, thickness effect and fluctuating Reynolds stresses in terms of a ghth component of the inflow distortion.

3.1 Acoustic Radiation from Periodic Blade Loading

Let us consider an element of span dr located at radius r on the jth blade and subjected to ghth component of inflow distortion described in subsection 2.1.1. Since the velocity fluctuations normal to the blade chord have the dominant influence on the lift fluctuations, it is sufficient to examine the influence of $U_{gh,\perp}$ described by Eq. (2.3). The lift per unit span of the blade given by Eq. (2.10) will be then periodic due to the periodic fluctuations of the incidence angle met by the blade, and can be related to its amplitude and the Sears' lift response function[8]. Denoting the blade that crosses the reference meridional plane at time t = 0, as the "first" blade, we can express the fluctuating lift on the jth blade element as

$$L_{gh,j} = \hat{L}_{gh} \cdot \exp\{-i(\omega_h - g\Omega)t + ig\Omega\tau_j + i\phi_{gh}\} \qquad (3.1)$$

where $\hat{L}_{gh} = \rho_o \pi V_r c \cdot \hat{U}_{gh,1} \cdot |S(\gamma)|$

$S(\gamma)$ = Sears' lift response function

and γ = reduced frequency = $(\omega_h - g\Omega) \frac{c}{2V_r}$

In the above representation the phase angle ϕ_{gh} includes the phase angle of the ghth component of $U_{gh,1}$ as in Eq. (2.3) and also the phase angle in the Sears' function $S(\gamma)$. We note that $\hat{L}_{gh}$ and ϕ_{gh} are not subscripted by j since all the blade elements at radius r and the flow conditions met by them are assumed identical. However, the lift fluctuations on the jth blade element occur at time τ_j earlier than those on the first blade, where

$$\tau_j = \frac{j-1}{B\Omega} \cdot 2\pi \tag{3.2}$$

Denoting the point of application of the force $L_{gh,j}$ by ζ'_{gh}, measured along the blade chord from its midchord location, we can use Eqs. (2.11) and (2.12) to obtain its coordinates, as

$$x_j = -\zeta'_{gh} \cos\lambda$$

$$r_j = r$$

and

$$\theta_j = \Omega t + (j-1)2\pi/B - \frac{\zeta'_{gh} \sin\lambda}{r} \tag{3.3}$$

We note that the location ζ'_{gh} on the blade chord is not subscripted by j, since all the blades are considered identical.

Considering the lift force as concentrated at the point defined by its coordinates given in Eq. (3.3), we can employ complex Fourier series representation to obtain the force over an elemental area $r d\theta\, dr$ at $(-\zeta'_{gh} \cos\lambda, r, \theta)$ as

$$\delta L_{gh,j} = \frac{\hat{L}_{gh}}{2\pi} \sum_{m} \exp\{-i(\omega_h - g\Omega + m\Omega)t + im\theta + i\phi_{gh}$$

$$+ im(\zeta'_{gh} \sin\lambda)/r - i(m-g)(j-1)2\pi/B\}\, dr\, d\theta \qquad (3.4)$$

We note that $\delta L_{gh,j}$ denotes the contribution due to lift on the jth blade element and its motion in a circle with rotational frequency Ω. Sound pressure at the far field point due to the fluctuating force described above can be obtained as

$$\delta p^{d}_{gh,j} = \frac{1}{4\pi S a_o}\left[\frac{\partial}{\partial t}\{(-\sin\lambda\cos\Psi + \cos\lambda \sin\theta_j \sin\Psi)\cdot\delta L_{gh,j}\}\right] \qquad (3.5)$$

where the square bracket indicates that the derivative is evaluated at retarded time $t - S/a_o$, and S is the distance of the field point from source located at coordinates $(-\zeta'_{gh}\cos\lambda, r, \theta)$. Substitution of Eq. (3.4) into the above is carried out in section A2 of the appendix, resulting in Eq. (A2.1) for $\delta p^{d}_{gh,j}$. Considering the loading on all the blade elements contained in the fan annulus, we obtain the far field acoustic pressure as

$$p^{d}_{gh} = \int_{r_h}^{r_t} \int_{0}^{2\pi} \sum_{j=1}^{B} \delta p^{d}_{gh,j} \qquad (3.6)$$

The superscript d and the subscript gh on the left hand side of Eq. (3.5) and (3.6) denote that the expression is for the contribution from dipole radiation from the effect of the ghth component of the inflow distortion. After completing the integration over θ and summation over j in the above equation, it is shown in section A2 of the appendix that sound radiation

at blade passing frequency occurs only when $\omega_h = 0$, i.e. for steady state inflow distortion. Integration over r can be simplified in terms of the value of the integrand at a representative radius r_e and it is shown in section A.2 of the appendix that the rms value of the nth harmonic of the far field sound pressure given by Eq. (3.6) reduces to

$$\tilde{p}^{d}_{gn} = \frac{K_{nB}}{4\sqrt{2}\pi R} \cdot B\hat{L}_g \cdot f_{\lambda e} \cdot J_m(K_{nB} r_e \sin\Psi) \cdot (r_t - r_h) \qquad (3.7)$$

where $K_{nB} = nB\Omega/a_o$

$m = nB + g$

$f_{\lambda_e} = \sin\lambda_e \cos\Psi - \frac{m}{K_{nB} r_e} \cos\lambda_e$

and $\hat{L}_g$ = amplitude of periodic blade loading defined in Eq. (3.1) for $\omega_h = 0$, evaluated at $r = r_e$.

We note that the harmonic index n in the above equation takes on both positive and negative integer values, and the absolute value of the right hand side is implied. The index g also takes on both positive and negative integer values according to Eq. (2.3) describing the inflow distortion. When a rotor is subjected to a known inflow distortion, the resulting sound pressure can be obtained by summing over g, the result of Eq. (A2.6), taking into account the amplitude and phase angle of each gth component, before taking the rms value. To indicate the possibility of high levels of blade passing frequency noise from the small scale fan, we substituted into Eq. (3.7) the blade loading $\hat{L}_g$ corresponding to $\hat{U}_{g,1} = 0.01 U_a \sin\lambda_e$ with $U_a = 83.5$ ft/sec, for all values of

the index g, and $r_e = \frac{1}{2}(r_h + r_t)$. For each value of g the results obtained for n = +1 and -1 from Eq. (3.7) are added to give the sound pressure at the blade passing frequency. The results of our computations for $|g|$ from 6 to 15 are shown in Fig. 3.1. For values of $|g|$ less than 6, the sound pressure levels computed are too low to be shown in the figure. Computations for $|g|$ between 15 and 24 were not carried out, but an examination of Eq. (3.7) indicates that the results could be comparable to those presented in Fig. 3.1 when the correspondence of the values of m is recognized. However, as $|g|$ increases the blade loading $\hat{L}_g$ is reduced and also the directivity would be affected due to the second term in f_{λ_e}.

It is interesting to note that even a small amplitude of the gth component of inflow distortion can yield considerable radiated sound pressure, as the value of g is increased. However, the inflow distortion over the rotor annulus has to be quite large to yield the amplitude of one percent of axial flow for the gth component used in our acoustic computations, as the value of g is increased.

The special case of acoustic radiation from the rotor blades operating in uniform axial flow can be obtained by replacing $\hat{L}_g$ in Eq. (3.7) by the steady state blade lift L_o Hence, for the rotor in uniform axial inflow we have

$$\tilde{p}_n^d = \frac{K_{nB}}{4\sqrt{2}\pi R} \cdot BL_o \cdot f_{\lambda_e} \cdot J_{nB}(K_{nB}\, r_e \sin\Psi) \cdot (r_t - r_h) \qquad (3.8)$$

where $L_o = \frac{1}{2} \rho_o V_r^2 C_L c$, evaluated at $r = r_e$ (3.9)

and n takes on both positive and negative values.

Gutin[9], nearly four decades ago, investigated noise from a rotor in uniform flow and the above equation for tone noise is in agreement with his results. In carrying out acoustic computations on the small scale fan according to above Eq. (3.8), we used $U_a = 83.5$ ft/sec and $C_L = 0.3$, in view of the lightly loaded condition of the rotor blades. The results of such computations are shown in Fig. 3.2 and these theoretical estimates are several orders of magnitude lower than test data as can be expected from multibladed rotors.

3.2 Effect of Blade Thickness

The distribution of volume sources along the chord of the jth blade to account for the blade thickness is described by Eq. (2.14) derived in subsection 2.3. In the presence of inflow distortion, the relative velocity V_r met by the blade element, traveling along the circumference $2\pi r$, will be a function of time with its ghth component defined by Eq. (2.4). Consequently, we can replace Eq. (2.14) by

$$q_{gh,\zeta j} = \frac{db}{d\zeta} \cdot d\zeta \, dr \cdot \hat{U}_{gh,r} \cdot \exp\{-i(\omega_h - g\Omega)t + ig\Omega\tau_j + i\phi_{gh}\} \quad (3.10)$$

where ϕ_{gh} represents the phase angle of $U_{gh,r}$ and τ_j represents the time lag with respect to the "first" blade as given by Eq. (3.2). We note that the various functions on the right hand side are not identified with subscript j since all the

blades are considered identical, except for time delay accounted by τ_j. The location of the periodic volume source described above is given by Eq. (2.15) of the preceeding section. By using complex Fourier series representation of the above volume source at its coordinates, the "monopole" per unit volume $d\zeta\, dr\, rd\theta$ can be obtained as

$$\delta q_{gh,\zeta j} = \frac{\hat{U}_{gh,r}}{2\pi} \frac{db}{d\zeta} d\zeta\, dr\, d\theta \sum_m \exp\{-i(\omega_h - g\Omega + m\Omega)t + i\phi_{gh} + im(\zeta \sin\lambda)/r - i(m-g)(j-1)2\pi/B\} \tag{3.11}$$

We note the above expression is for the contribution from the volume source $q_{gh,\zeta j}$ at ζ on the chord of the jth blade, due to the effect of the ghth component of the inflow distortion.

The far field acoustic pressure due to the elemental volume source, described above and located at $(-\zeta \cos\lambda, r, \theta)$ can be written as

$$\delta p^s_{gh,\zeta j} = \frac{\rho_o}{4\pi S} \left[\frac{\partial}{\partial t} \delta q_{gh,\zeta j} \right] \tag{3.12}$$

where the square bracket denotes that the derivative is evaluated at retarded time $(t - S/a_o)$. Substitution of Eq. (3.11) into the above, and application of the far field approximations are given in section A4 of the appendix. By including the volume sources distributed over the chord of each blade element and all the blade elements in the fan annulus, we obtain the far field sound pressure due to the ghth component of inflow distortion as

$$p^s_{gh} = \int_{r_h}^{r_t} \int_{0}^{2\pi} \sum_{j=1}^{B} \int_{-c/2}^{c/2} \delta p^s_{gh,\zeta j} \qquad (3.13)$$

After integrating over θ, and summing over j, it is shown in section A4 of the appendix that tone noise at blade passing frequency exists only when $\omega_h = 0$, i.e. for steady state inflow distortion. In terms of the representative radius r_e, the rms value of the nth harmonic of sound pressure given by Eq. (3.13) is derived in the appendix as

$$\tilde{p}^s_{gn} = \frac{\rho_o nB\Omega}{4\sqrt{2}\pi R} \cdot \hat{U}_{g,r} \cdot B \cdot G_{mge} \cdot J_m(K_{nB}\, r_e\, \sin\Psi) \cdot (r_t - r_h) \qquad (3.14)$$

where $K_{nB} = nB\Omega/a_o$

$m = nB + g$

and $$G_{mge} = \int_{-c/2}^{c/2} \frac{db}{d\zeta} \cdot \exp\{im(\zeta \sin\lambda)/r + iK_{nB}(\zeta \cos\lambda)\cos\Psi\} \cdot d\zeta \;;\; \text{at } r = r_e \qquad (3.15)$$

We observe that evaluation of sound pressure according to the above Eq. (3.14) for the effect of blade thickness is complicated since the function G_{mge} has to be obtained at each azimuth angle and harmonic index n, for a given blade profile. As a typical example we considered a double-circular arc profile with 10% thickness ratio and the evaluation of G_{mge} is described in section A4 of the appendix.

In carrying out acoustic computations on the small scale fan as per above Eq. (3.14), we employed $\hat{U}_{g,r} = 0.01\, U_a \cos\lambda_e$ with $U_a = 83.5$ ft/sec for all values of $|g|$ from 6 to 15, and

the resulting sound pressure levels are shown in Fig. 3.3. The influence of $|g|$ is to some extent similar to that discussed in the preceeding subsection. We observe that the blade thickness effect can be comparable to that of blade loading, in the prediction of rotor noise due to inflow distortion.

For the case of the rotor in uniform axial inflow, Eq. (3.14) reduces to

$$\tilde{p}_n^s = \frac{\rho_o nB\Omega}{4\sqrt{2}\pi R} \cdot V_r B \cdot G_{nBe} \cdot J_{nB}(K_{nB} r_e \sin\Psi) \cdot (r_t - r_h) \qquad (3.16)$$

where G_{nBe} = integral of Eq. (3.15) with m = nB.
Results of computations according to above equation for the design operating conditions of the small scale fan are shown in Fig. 3.4, and we observe that these predicted values also are several orders of magnitude lower than test data, indicating that consideration of uniform axial inflow leads to insignificant noise levels.

3.3 Quadrupole Radiation from Fluctuating Reynolds Stresses

Our primary interest in the present investigation is on the noise source in a rotor that can give rise to the high tone levels measured at on-axis point. Consequently, we limited our attention only to the longitudinal axial quadrupoles, by setting i = j = 1 in Eq. (2.16) for the stress tensor. The far field acoustic pressure from such elemental quadrupole can be written as

$$\delta p^q = \frac{\cos^2\psi}{4\pi a_o^2 S}\left[\frac{\partial^2}{\partial t^2}\left(\rho_o V_1 V_1\right)\right] \cdot d\,vol \tag{3.17}$$

where the square bracket denotes that the derivative is evaluated at retarded time $t - S/a_o$.

Since we are interested only in the consequences of a ghth component of inflow distortion, the axial component V_1 in the region upstream of the rotor can be written as

$$V_1 = U_{gh,1} + U_{p,1} \tag{3.18}$$

where $U_{gh,1}$ can be described in terms of its amplitude and phase angle in a manner similar to Eq. (2.3) or (2.4) and $U_{p,1}$ is described by Eq. (2.5). Considering the time derivative in Eq. (3.17), we observe that tone noise at harmonics of blade passing frequency would occur only when $\omega_h = 0$ and we can substitute

$$\rho_o V_1 V_1 = 2\rho_o \hat{U}_{g,1} \cdot \hat{U}_{p1,n} \cdot \exp\{i(g\theta + \theta_g) - |2n\pi\eta_1/d| + inB(\theta - \Omega t) + i\phi_{p1,n}\} \tag{3.19}$$

into Eq. (3.17) to obtain the nth harmonic of the blade passing frequency of δp^q. By including the radiation from all the quadrupoles present in the region upstream of the rotor, we obtain

$$p^q_{g,n} = \int_r \int_\theta \int_{\eta_1} \delta p^q_n \; r\,dr\,d\theta\,d\eta_1 \tag{3.20}$$

Substitution of Eq. (3.19) into Eq. (3.17) to obtain the nth harmonic δp^q_n and the details of integration are given in section A.6 of the appendix. From Eq. (A6.2) for $p^q_{g,n}$ we can

obtain its rms value as

$$\tilde{p}^{q}_{g,n} = \frac{\rho_o K_{nB}}{4\sqrt{2}\pi R} \cdot \cos^2\Psi \cdot \frac{d_e}{|n|} \cdot \; 2\hat{U}_{g,1}\, \hat{U}_{p_1,n} \cdot J_m(K_{nB} r_e \sin\Psi)$$

$$X\; r_e(r_t - r_h) \qquad (3.21)$$

where $m = nB + g$

and $K_{nB} = nB\Omega/a_o$.

We note that the above equation is a result of considering only the longitudinal axial quadrupoles, and for azimuth angles $\Psi \neq 0$, one should include the effects of $U_{p_3,n}$ and $U_{g,3}$ also. Consequently any comparison of the above result with the corresponding value for dipole radiation from blade loading can be made only for on-axis point.

In evaluating the sound pressure at on-axis points from Eqs. (3.7) and (3.21), we note that

$$g = -nB$$

Using the approximate expression

$$|S(\gamma)| = \left|\frac{\pi nB\Omega c}{V_r}\right|^{-\frac{1}{2}}$$

for Sears' lift response function to obtain $\hat{L}_g$ for substitution into Eq. (3.7), we obtain

$$\left\{\tilde{p}^{q}_{gn} / \tilde{p}^{d}_{gn}\right\}_{\text{at } \Psi=0} = 2\sqrt{2} \cdot \frac{|n|}{\sigma} \cdot M_r \left\{\frac{\hat{U}_{g,1}\; \hat{U}_{p_1,n}}{\hat{U}_{g,1}\; V_r}\right\} (\sin\lambda_e)^{\frac{1}{2}} \qquad (3.22)$$

The above ratio denotes the relative importance of the quadrupole radiation in estimating on-axis noise from rotors in distorted inflow. Even though $g = -nB$ for the gth component of inflow distortion in evaluating the on-axis noise, we

retained both the subscripts g and n in the above equation. We note that all other factors except $M_r \cdot (\hat{U}_{p_1,n}/V_r)$ and the harmonic index n can be of the order one in most fan designs including the small scale fan. Substituting the value for $\hat{U}_{p_1,n}$ estimated on the small scale rotor in reference 3, we find that the ratio given by Eq. (3.22) is low. Hence, further consideration of quadrupole radiation from the small scale rotor in distorted inflow is ignored. However, for evaluating tone noise at higher harmonics from fans with blades operating at $C_L \simeq 1.0$ and $M_r \simeq 1.0$, the quadrupole radiation cannot be ignored.

4.0 DISCRETE TONE NOISE FROM ROTOR INTERACTIONS WITH INFLOW TURBULENCE

The effect of turbulence in the inflow to the rotor is to cause random fluctuations in the relative velocity and the incidence angle met by each blade element as it travels around the rotor circumference. Even though the events occurring on each blade element are random in nature, the analyses presented in the following two subsections show that discrete tones can appear in the spectrum of radiated noise from the rotor. These discrete tones occurring at the blade passing frequency and its harmonics are caused by the low frequency fluctuations of the turbulent inflow, which in turn are related to the longitudinal length scale in the frozen convected model used in our analysis. Because of the periodicity of the rotor-induced velocity fluctuations, quadrupole radiation from the fluctuating Reynolds stresses also gives rise to discrete tone noise as discussed in the last subsection.

4.1 Effect of Random Blade Loading

The fluctuating lift on a blade element is related to the fluctuations of u_1 , the turbulent velocity component normal to the blade chord. The latter, being a stationary random function of time with zero mean, can be represented by means of a Fourier-Stieltjes integral[10].

$$u_1(t) = \int_{\omega=-\infty}^{\infty} e^{-i\omega t} \, dZ_{u_1}(\omega) \tag{4.1}$$

where $Z(\omega)$ is a non-differentiable random function, and its power spectral density is given by

$$\overline{dZ_{u_1}(\omega) \cdot dZ^*_{u_1}(\omega')} = \Phi_{u_1}(\omega) \cdot \delta(\omega - \omega') \cdot d\omega \, d\omega' \qquad (4.2)$$

Although u_1 is a random function of time and space, it has coherency over a certain volume in space, called the eddy volume. Let us assume that u_1 is perfectly correlated over a circumferential length ℓ_3. Since this velocity pattern repeats itself in the θ direction with period 2π, we can write for the velocity fluctuation at any θ location due to the influence of one particular eddy located at θ_0 and radius r, as

$$u_1(r,\theta,t) = \sum_g A_g e^{ig(\theta-\theta_0)} \int_{\omega=-\infty}^{\infty} e^{-i\omega t} \, dZ_{u_1}(\omega) \qquad (4.3)$$

where $A_g = \frac{1}{g\pi} \sin(g\ell_3/2r)$.

Since a blade element travels through angle $\theta = \Omega t$ during a time t, it experiences velocity fluctuations at circular frequency $(\omega - g\Omega)$. The fluctuating lift force per unit span on blade element of the "first" blade located at radius r is then given by

$$\Delta L_1 = \pi \rho_o V_r c \sum_g A_g e^{-ig\theta_0} \int_{\omega=-\infty}^{\infty} e^{-i(\omega-g\Omega)t} S(\gamma') dZ_{u_1}(\omega) \qquad (4.4)$$

where ΔL = the load due to random velocity fluctuations occurring in a coherent eddy, and the subscript *1* denotes the "first" blade,

$S(\gamma')$ = Sears' lift response function

γ' = reduced frequency = $(\omega - g\Omega) \frac{c}{2V_r}$.

Similar to the above Eq. (4.4), the load on the jth blade can be written as

$$\Delta L_j = \pi\rho_o V_r c \sum_g A_g \cdot \exp\{-ig(\theta_o - \Omega\tau_j)\} \times \int_{\omega=-\infty}^{\infty} e^{-i(\omega-g\Omega)t} S(\gamma')\, dZ_{u_i}(\omega) \qquad (4.5)$$

where $\tau_j = (j-1)2\pi/B\Omega$

is the phase difference from the loading on the "first" blade. At any time t, the location of the point of application of the force L_j on the jth blade element is defined by Eq. (2.11) given in the earlier subsection 2.2. Using complex Fourier series representation, as employed in deriving Eq. (3.4), the random lift load on an elemental area $r d\theta\, dr$ at $(-\zeta' \cos\lambda, r, \theta)$ due to the loading on the jth blade, can be written as

$$\delta L_j = \frac{\rho_o V_r c}{2} \sum_m \sum_g A_g \exp\{im\theta + im\zeta' \sin\lambda/r - ig\theta_o\} \times \exp\{-i(m-g)(j-1)\frac{2\pi}{B}\} \times \int_{\omega=-\infty}^{\infty} \exp\{-i(\omega - g\Omega + m\Omega)t\} S(\gamma')\, dZ_{u_i}(\omega)\, dr\, d\theta \qquad (4.6)$$

The acoustic pressure at the far field point due to the above impressed force can be obtained from

$$\delta p_j^d = \frac{1}{4\pi S a_o} \left[\frac{\partial}{\partial t} \{(-\sin\lambda \cos\Psi + \cos\lambda \sin\theta_j \sin\Psi) \cdot \delta L_j\} \right] \qquad (4.7)$$

where the square bracket indicates that the derivative is evaluated at retarded time $t - S/a_o$. Substitution of

Eq. (4.7) into the above, and far field approximation is given in section A3 of the appendix. After considering the loading on all the blade elements contained in the fan annulus, and the contribution from all independent coherent regions present in the fan annulus, the following expression is derived in the appendix for the spectrum of the far field sound pressure.

$$\Phi^{d}(\nu) = \frac{1}{2}\int_{r_h}^{r_t} (\pi\rho_o V_r c)^2 \cdot \left(\frac{\nu}{4\pi R a_o}\right)^2 \cdot \ell_2 \cdot \frac{2\pi r}{\ell_3} \cdot B^2$$

$$\times \sum_{m}\sum_{g} A_g^2 \cdot f_\lambda^2 \cdot J_m^2\left(\frac{\nu}{a_o} r \sin\Psi\right) \cdot \Phi_{u_\perp}(\omega) \cdot |S(\gamma')|^2 \cdot dr \qquad (4.8)$$

where $\Phi_{u_\perp}(\omega) = \overline{u^2}(\ell/\pi U_a)\{1 + (\ell\omega/U_a)^2\}^{-1}$

$\omega = \nu - nB\Omega$; $m = nB + g$; $n = \ldots.-1,0,1\ldots\ldots$

$S(\gamma')$ = Sears' lift response function

$\gamma' = (\omega - g\Omega)(c/2V_r)$

and $f_\lambda = \sin\lambda \cos\Psi - (ma_o/\nu r)\cos\lambda$

It is to be noted that, in the representation employed in Eq. (4.3) the coefficient A_g can be zero for certain values of ℓ_3. This particular behavior of A_g is due to our assumption of a perfectly correlated eddy which of course is an oversimplification. Since the eddy size ℓ is not unique, instead of defining A_g as in Eq. (4.3), it is more appropriate to use the envelope function of A_g^2. A reasonable approximation to this envelope function is

$$A_g^2 = \{\frac{1}{g\pi} \sin(g\ell_3/2r)\}^2 \quad \text{for} \quad |\frac{g\ell_3}{2r}| < \frac{\pi}{2}$$

and $A_g^2 = \{(\ell_3/2\pi r)(1 + g\ell_3/2r)\}^2\{1 + (g\ell_3/2r)^2\}^{-2}$ otherwise (4.9)

In carrying out acoustic computation on the small scale fan, the integration over r in Eq. (4.8) is approximated by considering the value of the integrand at an effective radius r_e, as in the previous section 3. Assuming 3% turbulence intensity and parametric values of ℓ/d_e ratio, the sound spectra at an axis point 5 ft. from rotor are computed, and the results are given in Fig. 4.1. As the turbulence length scale is increased, the spectra show prominent peaks at blade passing frequency and its higher harmonics. We note that there are no spurious peaks in the spectrum obtained with the present approach as compared with that reported in reference 11, wherein perfect correlation of loading on a finite number of blades was assumed. The function of β_1, the number of blades "chopping" an eddy, as postulated in reference 11, was responsible for the series of less prominent peaks seen in the noise spectra. In the present approach, we considered all the rotor blades, but only that part of the loading caused by velocity fluctuations in a coherent eddy.

Directivity patterns of radiated acoustic pressure at blade passing frequency and its first harmonic, calculated for the case of $\ell/d_e = 5.0$ are presented in Fig. 4.2, and indicate that the noise on the side line can be 10 dB lower than that along the axis.

Computations carried out by Mani[12] for acoustic power radiated from a rotor interacting with inflow turbulence indicate discrete tones at blade passing frequency, and higher harmonics, similar to the results presented here. However, the peaks in the spectra presented in fig. 4.1 are much sharper than the results given in reference 12, possibly due to the differences in the assumption of loading occurring on the blades. Recently, Homicz and George[13] presented an analysis of acoustic radiation from rotors in turbulent flow. Their results also do not show, probably for the same reasons as indicated above, the sharpness of the discrete tones evident in the narrow band analysis of experimental measurements.

4.2 Effect of Blade Thickness

The strength of the volume sources distributed along the blade chord to represent the thickness effect depend upon the relative velocity met by the blade as discussed in the earlier subsection 3.2. Let us consider the consequences of the random nature of these volume sources resulting from the turbulent fluctuation in the inflow to the rotor.

Similar to Eq. (4.1) we can represent u_r , the fluctuating velocity component along the mean relative velocity direction as

$$u_r = \int_{\omega=-\infty}^{\infty} e^{-i\omega t} \, dZ_{u_r}(\omega) \qquad (4.10)$$

and replace V_r in Eq. (2.14) by the above expression to obtain the random fluctuation of the elemental volume source $q_{\zeta j}$ located at ζ on the chord of the jth blade. Using the same approach as employed in the preceeding subsection, we obtain the randomly fluctuating volume source distribution, due to the velocity fluctuations in a coherent eddy, as

$$\delta q_{\zeta j} = \frac{1}{2\pi} \sum_m \sum_g A_g \cdot \exp\{im\theta + im\zeta \sin\lambda/r - ig\theta_o\}$$
$$\times \exp\{-i(m-g)(j-1)\frac{2\pi}{B}\}$$
$$\times \int_{\omega=-\infty}^{\infty} \exp\{-i(\omega - g\Omega + m\Omega)t\} \cdot \frac{db}{d\zeta} d\zeta\, dr\, d\theta \cdot dZ_{u_r}(\omega) \qquad (4.11)$$

Acoustic radiation from above random volume source distributuion can be calculated from

$$\delta p^s_{\zeta j} = \frac{\rho_o}{4\pi S} \left[\frac{\partial}{\partial t} \delta q_{\zeta j}\right] \qquad (4.12)$$

where the square bracket is used in the same sense as in Eq. (4.7). The substitution of Eq. (4.11) into Eq. (4.12) is shown in section A5 of the appendix and the acoustic spectrum due to radiation from all the blades in the fan annulus is given by

$$\Phi^s(\nu) = \frac{1}{2} \int_{r_h}^{r_t} \left\{\frac{\nu\rho_o}{4\pi R}\right\}^2 \cdot \ell_2 \cdot (2\pi r/\ell_3) \cdot B^2$$
$$\times \sum_m \sum_g A_g^2 \cdot |G_{mge}|^2 \cdot \Phi_{u_r}(\omega) \cdot J_m^2(\frac{\nu}{a_o} r \sin\Psi) dr \qquad (4.13)$$

where $\Phi_{u_r}(\omega)$ = spectrum of u_r as defined by Eq. (2.8)

$\omega = \nu - nB\Omega$

$m = nB + g$

A_g^2 = function defined in Eq. (4.9)

and $$G_{mge} = \int_{-c/2}^{c/2} \left(\frac{db}{d\zeta}\right) \exp\{im\zeta \sin\lambda/r + i \frac{\nu}{a_o} \zeta \cos\lambda \cos\Psi\} \cdot d\zeta$$ evaluated at $r = r_e$ (4.14)

In carrying out acoustic computations on the small scale fan as per above Eq. (4.13), we employed the same turbulence parameters as used in subsection 4.1. The integral in Eq. (4.14) is evaluated for the same blade profile used in the computations presented in subsection 3.2. The computed spectra presented in Fig. 4.3 also show prominent peaks at blade passing frequency and its higher harmonics but the levels are much lower than those given in Fig. 4.1, for the blade loading effects. The directivity patterns of tone noise at the blade passing frequency and its first harmonic, as computed from Eq. (4.13) are shown in Fig. 4.4.

Computational results presented in this subsection indicate that blade thickness effect can be important at higher harmonics of the blade passing frequency.

4.3 Radiation from Random Quadrupole Sources

In the region upstream of the rotor leading edge there exist periodic velocity fluctuations, as discussed in subsection 2.1.2, in addition to the random turbulent velocity fluctuations of the inflow described in subsection 2.1.3.

Since our primary interest is to evaluate such sources that would yield acoustic radiation to on-axis points, we shall consider only the longitudinal axial quadrupoles as in subsection 3.3. For random quadrupole calculations, instead of using Eq. (3.17), it is more appropriate to obtain the spectrum of the far field acoustic pressure by integrating the space-time correlation of the fluctuating Reynolds stresses over the flow region, as indicated in reference 14. Thus, the far field sound spectrum due to the longitudinal axial quadrupoles can be written as

$$\Phi_p^q(R,\nu) = \frac{\rho_o^2 \cos^4\Psi}{(4\pi a_o^2 R)^2} \frac{\nu^4}{2\pi} \int_\infty d^3\underset{\sim}{\eta} \int_\infty d^3\underset{\sim}{\xi} \int_\infty R(\underset{\sim}{\eta},\underset{\sim}{\xi},\tau) \cdot \cos(\tau - \tau^*) d\tau \tag{4.15}$$

where $R(\eta,\xi,\tau) = \overline{V_1^2(\underset{\sim}{\eta},t) V_1^2(\underset{\sim}{\eta}+\underset{\sim}{\xi},\ t+\tau)}$ (4.16)

V_1 = axial component of V described in Eq. (2.1)

and $\tau^* \simeq \underset{\sim}{\xi}\cdot\underset{\sim}{R}/a_o R$ is the retarded time difference.

The position vector $\underset{\sim}{\eta}$, the separation vector $\underset{\sim}{\xi}$, and the region of integration are schematically shown in Fig. 4.5. In considering the tone noise of the quadrupole radiation due to inflow turbulence and rotor induced potential velocity fluctuations, we need to retain only the product term $2U_{p_1} u_1$ of V_1^2 in Eq. (4.16). The derivation of the space-time correlation function and the limits of integration are discussed in detail in section A7 of the appendix. After certain amount of algebraic simplification, the spectrum of far field acoustic pressure due to radiation from quadrupole sources can be written as

$$\Phi^{q}_{pn}(\nu) = \left\{\frac{\rho_o \nu^2}{4\pi a_o^2 R_o}\right\}^2 \cdot \cos^4\psi \cdot \frac{A(\Phi_1 - \Phi_2)\ell^4 \cdot (\overline{u^2}) \cdot (\hat{u}_{p_1,n})^2}{\{(k_p\ell/2)^2 + 1\}\{(k_p\ell)^2 - 1\}} \tag{4.17}$$

where

A = fan annulus area

$$\Phi_1 = \frac{U_a}{\pi\ell}\left\{\frac{1}{(U_a/\ell)^2 + (\omega_p - \nu)^2} + \frac{1}{(U_a/\ell)^2 + (\omega_p + \nu)^2}\right\}$$

$$\Phi_2 = \frac{U_a}{\pi\ell}\left\{\frac{1}{(U_a k_p)^2 + (\omega_p - \nu)^2} + \frac{1}{(U_a k_p)^2 + (\omega_p + \nu)^2}\right\}$$

$k_p = n2\pi/d$, $\omega_p = nB\Omega$.

For the same turbulence parameters, employed in calculating the results given in Fig. 4.1, we evaluated the quadrupole radiation to the on-axis point from the above equation, using the fundamental of the rotor-related potential velocity fluctuations. The resulting spectra presented in Fig. 4.6 peak at blade passing frequency, and once again the sound pressure levels are far below the corresponding values shown in Fig. 4.1 for radiation from blade loading. The spectra shown in Fig. 4.6 peak only at the blade passing frequency, since the fundamental component of U_{p_1} was considered. Based on his computations for tone power estimates at blade passing frequency, Chandrashekhara[15] also reached similar conclusions.

We observe that on the right hand side of Eq. (4.17), the dominant influence is from the first term of Φ_1, which can be recognized as the inflow turbulence spectrum shifted to

the frequency ω_p. This feature of quadrupole radiation due to inflow turbulence was also noted by Williams and Hawkings[16]. The various other terms containing k_p, not discussed in reference 16, appear in the above equation due to the exponential decay of $\hat{U}_{p_1}$ with distance upstream of rotor and integration over the whole flow region. A comparison of the Eqs. (4.17) and (4.8) evaluated at on-axis points can be reduced to

$$\left\{\frac{\Phi^q}{\Phi^d}\right\}_{\text{at } \Psi = 0} = \frac{4M_r^2 \sin\lambda}{|n|\sigma} \left\{\frac{\hat{U}_{p_1,n}}{V_r}\right\} \tag{4.18}$$

Since $\hat{U}_{p_1,n}$ can never be larger than V_r, the on-axis tone noise from subsonic rotors in turbulent inflow is dominated by the dipole radiation at all harmonics.

5.0 EXPERIMENTAL MEASUREMENTS AND COMPARISON WITH THEORETICAL PREDICTIONS

In the experiments conducted by NASA, Ames Research Center, the small scale rotor, whose design parameters were employed in the acoustic computations presented in the preceeding sections, is located at the center of the anechoic chamber and the exit flow from the fan is vented out of the chamber to avoid recirculation into the rotor inlet. Flow measurements, taken with the hot-wire located in the fan entrance bell-mouth at the pitch radius, and 6 in. upstream of the rotor, indicate a mean axial flow of 83.5 ft/sec and turbulence intensity of 0.75%. The spectrum of the axial component of turbulence, obtained with a 50 Hz band-width, is shown in Fig. 5.1. From the autocorrelation function presented in Fig. 5.2, a longitudinal velocity correlation length scale of 20 inches is deduced.

In carrying out acoustic computations consistent with the test conditions we assumed "frozen-convected" turbulence hypothesis, with 83.5 ft/sec as the convection velocity to obtain the power spectrum of u_1 from Eq. (2.7). Based on the measurements reported by Chandrashekhara[15] on a small scale rotor of comparable size, we find that the length scale ℓ_3 in the circumferential direction can be much smaller than 20 inches. Consequently, we employed parametric values of ℓ_3 = 1, 2 and 3 inches along with the above mentioned spectrum for u_1 to compute the noise spectra, according to

Eq. (4.8), at 7 ft. distance along the axis. The results thus obtained for dipole radiation from blade loading, are shown in Fig. 5.3. The peak levels at blade passing frequency and its harmonic did not vary appreciably with ℓ_3 in the range examined. Similar results obtained from Eq. (4.13) for monopole radiation from blade thickness effect are shown in Fig. 5.4, indicating the minor role of blade thickness in rotor noise prediction at on-axis points. Based on the conclusions reached in preceeding section regarding the relative unimportance of noise from the quadrupole sources, computations using Eq. (4.17) were not carried out for the test configuration.

The noise measured at 7 ft. distance from the rotor, along its axis, is analyzed using a 50 Hz bandwidth. The resulting spectrum, shown in Fig. 5.5, contains sharp peaks at the blade passing frequency and its first harmonic. For correlation with theoretical estimates, we note that the latter are computed from the sound pressure spectrum given by Eq. (4.8), which is derived for both positive and negative values of radian frequency. Hence, the acoustic pressure spectral density per Hertz for positive frequencies is obtained by using a multiplying factor of 4π to the results of Eq. (4.8). The spectral density thus obtained is integrated over 50 Hz bandwidth before finding the dB level for comparison with the measured values. Using length scale ℓ_3 = 3 inches, we carried out such calculations in the neighborhood of the blade passing frequency and its first harmonic and the theoretical estimates are shown by dotted lines

in Fig. 5.5. The change in the scale of the abscissa and integration over the 50 Hz bandwidth are responsible for the difference in estimated sound pressure levels presented in Fig. 5.5 and those shown in Fig. 5.3. It appears that the sharpness of the discrete tones observed in the test data is predictable from the theory presented here. Variability of the measured tone levels obtained with a 50 Hz bandwidth filter centered at the blade passing frequency and its first harmonic are shown in Fig. 5.6. Our theoretical predictions of the tone levels indicated by the dotted lines in Fig. 5.6 appear to be in reasonable agreement with the measured values.

The variability of the tone level, with time as seen in Fig. 5.6, can have its origin in the very nature of the noise sources. An examination of Eq. (4.8) with $\Psi = 0$, indicates that the tone noise level is proportional to the mean square value of turbulent velocity fluctuations at the low end of the spectrum. On the other hand, the data presented in Fig. 5.6 is obtained using a short averaging time-constant in view of the high frequencies of the tones. Consequently, the low frequency nature of the generation mechanism appears in the output as variability of the tone level.

The inlet to the rotor is not yet surveyed to assess the steady state distortion of the inflow. Hence, no estimates can be made at the present time for the on-axis noise from the ordered sources discussed in section 3.

6.0 CONCLUSIONS AND RECOMMENDATIONS

The theoretical investigations of noise sources in a rotor and typical computational results presented in this report lead us to the following observations:

(a) Steady state distortion of inflow, even of small magnitude, can generate high levels of noise at blade passing frequency harmonics.

(b) Periodic inflow distortions lead to tones at frequencies other than the blade passing frequency harmonics.

(c) The interaction of the rotor blades with inflow turbulence gives rise to noise whose spectrum contains prominent peaks at blade passing frequency and its higher harmonics. The sharpness and level of these discrete tones depend upon the intensity of turbulence and its velocity correlation length scale.

(d) Computations presented in this report indicate that the discrete tone level increases as the ratio ℓ/d is increased. Since blade speed V_t and the axial velocity U_a through the rotor are held constant in our computations, increased value of ℓ/d can be interpreted as more blades "chopping" a coherent eddy as it is convected across the rotor.

(e) Theoretical investigations show that the origin of the discrete tone noise lies in the turbulent velocity fluctuations at the low-end of frequency spectrum.

(f) Limited computations for the effect of inflow turbulence on the small scale rotor indicate that blade loading fluctuations are the dominant sources of noise in isolated rotors.

It is necessary to include the acoustic radiation from all the quadrupole sources and also the influence of the duct to make a rational comparison of the various noise sources in a rotor.

The analyses of noise sources and radiation therefrom, presented in this report, are applicable to rotor blades operating at relative Mach numbers in the low subsonic range. To evaluate noise from lift fans of present day configurations, the analyses must be extended to the consideration of high relative flow Mach numbers.

Space-time correlation measurements of inflow turbulence for various inlet configurations are recommended to determine the characteristics of turbulent velocity fluctuations. Such flow measurements along with corresponding acoustic data would confirm the assumptions employed in the present analysis and provide a basis for further improvements in the theoretical prediction of rotor noise.

From the preliminary investigation of noise sources presented here it appears that reduction of discrete tone noise from rotors can be achieved by eliminating inflow distortion and decreasing the length scale of the turbulent velocity fluctuations.

APPENDIX

The steps involved in deriving the expressions for the far field acoustic radiation from a rotor subjected to various inflow conditions are given in detail in the following sections of this appendix.

A1 Coordinate System and Distance to Far Field

Let $\underset{\sim}{R}$ and $\underset{\sim}{S}$ denote the vector distance of the far field point from the origin and source respectively as shown in Fig.2.1. For the sake of convenience and considering the cylindrical symmetry of the radiated field, we have chosen the meridional plane $\theta = 0$ to pass through the field point. By appropriate translation and rotation of the coordinate system, we can obtain the components of $\underset{\sim}{S}$ in the axial, radial and circumferential directions as

$$\begin{aligned} S_1 &= R\cos\Psi - x \\ S_2 &= R\sin\Psi\cos\theta - r \\ S_3 &= -R\sin\Psi\sin\theta \end{aligned} \qquad \text{(A1.1)}$$

The distance of the field point from the source location can be approximated as

$$S = R - r\sin\Psi\cos\theta - x\cos\Psi \qquad \text{(A1.2)}$$

In the far field computations of fan noise the second order terms r/R and x/R can be ignored in the amplitude decay term but not in the retarded time function.

A2 Dipole Radiation from Periodic Blade Loading

Substituting Eq. (3.4) into Eq. (3.5) and using Eq. (A1.2) for the far field approximation with the corresponding values of x_j and θ_j from Eq. (3.3), we obtain the following equation for acoustic radiation from an elemental area $rd\theta\, dr$ of the rotor disc

$$\delta p^d_{gh,j} = \frac{\hat{L}_{gh} \cdot dr d\theta}{2\pi} \sum_m \frac{iK_{mgh}}{4\pi R}(\sin\lambda \cos\Psi - \cos\lambda \sin\theta \sin\Psi)$$
$$\times \exp\{-iK_{mgh}a_o(t - R/a_o) + i\phi_{gh}\}$$
$$\times \exp\{im\theta - iK_{mgh} r \sin\Psi \cos\theta\}$$
$$\times \exp\{im(\zeta'_{gh} \sin\lambda)/r + iK_{mgh}(\zeta'_{gh} \cos\lambda)\cos\Psi\}$$
$$\times \exp\{-i(m - g)(j - 1)2\pi/B\} \qquad \text{(A2.1)}$$

where $K_{mgh} = (\omega_h - g\Omega + m\Omega)/a_o$

and λ = blade stagger, employed in obtaining axial and circumferential components of force L_{gh}.

On the left hand side of the above equation the subscript gh,j indicates that it is the contribution from the loading on the jth blade element due to its interaction with the ghth component of the inflow distortion. Considering the loading on all the blade elements contained in the fan annulus, we obtain the far field acoustic pressure as

$$p^d_{gh} = \int_{r_h}^{r_t} \int_0^{2\pi} \sum_{j=1}^{B} \delta p^d_{gh,j} \qquad \text{(A2.2)}$$

The superscript d and the subscript gh on the left hand side denotes that the expression is for the contribution from dipole radiation from the effect of only the ghth component of the inflow distortion. Substituting Eq.(A2.1) into Eq.(A2.2) and using the following identities

$$\int_0^{2\pi} \exp\{i(m\theta - z\cos\theta)\}d\theta = 2\pi(-i)^m J_m(z) \tag{A2.3}$$

$$\int_0^{2\pi} \sin\theta\cdot\exp\{i(m\theta - z\cos\theta)\}d\theta = \left(\frac{-m}{z}\right)2\pi(-i)^m J_m(z) \quad \text{and} \tag{A2.4}$$

$$\sum_{j=1}^{B} \exp\{-i(m-g)(j-1)2\pi/B\} = B, \text{ if } \frac{m-g}{B} = \text{an integer}$$
$$= 0 \text{ otherwise} \tag{A2.5}$$

we obtain the nth component of far field sound pressure as

$$p^d_{gh,n} = \int_{r_h}^{r_t} \frac{iK_{mgh}}{4\pi R}(-i)^m \exp\{-iK_{mgh}a_o(t - R/a_o) + i\phi_{gh}\}\cdot f_\lambda$$
$$\times \exp\{im(\zeta'_{gh}\sin\lambda)/r + iK_{mgh}(\zeta'_{gh}\cos\lambda)\cos\Psi\}$$
$$\times \hat{BL}_{gh}\cdot J_m(K_{mgh}r\sin\Psi)\cdot dr \tag{A2.6}$$

where $K_{mgh} = (\omega_h - g\Omega + m\Omega)/a_o$

$$f_\lambda = \sin\lambda\cos\Psi - \frac{m}{K_{mgh}\cdot r}\cos\lambda$$

and $m = nB + g$

We note that the frequency of the nth component of acoustic pressure defined above is

$$\frac{\omega_h + (m-g)\Omega}{2\pi} = \frac{\omega_h}{2\pi} + nBN\ , \tag{A2.7}$$

where N = rotor rps.

Consequently, sound radiation would occur at blade passing frequency only when $\omega_h = 0$, i.e. for steady state inflow distortion. By using a representative radius r_e and replacing the integrand of the above Eq. (A2.6) by its value at r_e, we can then write the rms value of the nth harmonic as

$$\tilde{p}^d_{gn} = \frac{K_{nB}}{4\sqrt{2}\pi R} \cdot B\hat{L}_g \cdot f_{\lambda e} \cdot J_m(K_{nB} r_e \sin\Psi) \cdot (r_t - r_h) \qquad \text{(A2.8)}$$

where $K_{nB} = nB\Omega/a_o$

and $\hat{L}_g$ = amplitude of periodic blade loading defined by Eq. (3.1) for $\omega_h = 0$.

A3 Dipole Radiation from Random Blade Loading

Substituting Eq. (4.6) into Eq. (4.7) and using Eq. (A1.2) for the far field approximation we obtain the following expression

$$\delta p^d_j = \frac{\rho_o V_r c}{2} \sum_m \sum_g A_g \int_{\omega=-\infty}^{\infty} \frac{iK_{mg}}{4\pi R} (\sin\lambda \cos\Psi - \cos\lambda \sin\theta \sin\Psi)$$

$$\times \exp\{-iK_{mg} a_o (t - R/a_o) - ig\theta_o\}$$

$$\times \exp\{im\theta - iK_{mg} r \sin\Psi \cos\theta\}$$

$$\times \exp\{im\zeta' \sin\lambda/r + iK_{mg} \zeta' \cos\lambda \cos\Psi\}$$

$$\times \exp\{-i(j-1)(m-g)2\pi/B\} S(\gamma') dZ_{u_\perp}(\omega) \, dr \, d\theta \qquad \text{(A3.1)}$$

where $K_{mg} = (\omega - g\Omega + m\Omega)/a_o$

$S(\gamma')$ = Sears' lift response function at reduced frequency γ,

and $\gamma' = (\omega - g\Omega) \frac{c}{2V_r}$

Now carrying out summation over j from 1 to B to account for the effect of all blades and integrating over $0 \leq \theta \leq 2\pi$ gives the far field acoustic pressure from blade elements within an annulus $2\pi r dr$ due to interactions with a coherent eddy as

$$\Delta p^d = \frac{\rho_o V_r cB}{2} \sum_m \sum_g A_g \int_{\omega=-\infty}^{\infty} \frac{iK_{mg}}{4\pi R} 2\pi(-i)^m$$

$$\times \exp\{-iK_{mg} a_o (t - R/a_o) - ig\theta_o\}$$

$$\times \exp\{im\zeta' \frac{\sin\lambda}{r} + iK_{mg} \zeta' \cos\lambda \cos\Psi\}$$

$$\times J_m(K_{mg} r \sin\Psi) \cdot f_\lambda \cdot S(\gamma') dZ_{u_1}(\omega) dr \qquad \text{(A3.2)}$$

where $m = nB + g$,

and $f_\lambda = \sin\lambda \cos\Psi - \frac{m}{rK_{mg}} \cos\lambda$

Noting that the dimension of the coherent eddy in the radial direction is ℓ_2 we can approximate the integration with respect to r by some mean value of Δp^d multiplied by ℓ_2 to obtain the far field acoustic pressure from blade elements within an annulus $2\pi r\ell_2$. It is to be noted that the value ℓ_2 in the above equation must be limited to $(r_t - r_h)$, since the loading on the blade elements is defined only within the fan annulus. The auto-correlation function of the acoustic pressure, thus obtained for interactions with a coherent eddy, leads to the spectral density by taking its Fourier transform. However, it is only the contribution from the interaction of the rotor blades with a coherent eddy. To

obtain the spectrum due to all coherent regions present in an annulus $2\pi r dr$, we can multiply the spectrum obtained as above by $2\pi r/\ell_3$ and dr/ℓ_2. The spectral density at circular frequency ν, of the radiated acoustic pressure from all the blade elements within the rotor annulus is then given by

$$\Phi^d(\nu) = \frac{1}{2}\int_{r_h}^{r_t} (\pi\rho_o V_r c)^2 \cdot (\frac{\nu}{4\pi R a_o})^2 \cdot \ell_2 \cdot \frac{2\pi r}{\ell_3} \cdot B^2$$

$$\times \sum_m \sum_g A_g^2 \cdot f_\lambda^2 \cdot J_m^2 (\frac{\nu}{a_o} r \sin\Psi)$$

$$\times \Phi_{u_1}(\omega) \cdot |S(\gamma')|^2 \cdot dr \qquad \text{(A3.3)}$$

where $\omega = \nu - m\Omega + g\Omega$; $m = nB + g$; $n = \ldots -1, 0, 1 \ldots\ldots$

and $\gamma' = (\omega - g\Omega)\frac{c}{2V_r}$, and other parameters are as defined in Eqs. (A3.1) and (A3.2).

A4 Monopole Radiation Due to Inflow Distortion

The effect of the ghth component of the inflow on the thickness of the jth blade rotating with a circular frequency Ω, is represented by fluctuating volume sources $\delta q_{gh,\zeta j}$, as given in Eq. (3.11). We note that the elemental volume $r d\theta\, dr\, d\zeta$ referred to in the equation is located, in the annulus $2\pi r dr$, at coordinates given by Eq. (2.15). Substituting Eq. (3.11) into Eq. (3.12) and using the far field approximations as before, we obtain the acoustic pressure due to the elemental monopole considered as

$$\delta p^{s}_{gh,\zeta j} = \frac{1}{2\pi}\,\hat{U}_{gh,r}\cdot\frac{db}{d\zeta}\cdot d\zeta\; dr\; d\theta \sum_{m}\left(\frac{-i\rho_o a_o K_{mgh}}{4\pi R}\right)$$

$$X\quad \exp\{-iK_{mgh}\, a_o(t - R/a_o) + i\phi_{gh}\}$$

$$X\quad \exp\{im\theta - iK_{mgh}\, r\sin\Psi\cos\theta\}$$

$$X\quad \exp\{im(\zeta\sin\lambda)/r + iK_{mgh}(\zeta\cos\lambda)\cos\Psi\}$$

$$X\quad \exp\{-i(m-g)(j-1)2\pi/B\} \qquad \text{(A4.1)}$$

where $K_{mgh} = (\omega_h - g\Omega + m\Omega)/a_o$

Including the source-sink distribution over the chord of each blade element and all the blade elements in the fan annulus, the far field sound pressure due to the ghth component of inflow distortion can be obtained from the following equation.

$$p^{s}_{gh} = \int_{r_h}^{r_t}\int_{o}^{2\pi}\sum_{j=1}^{B}\int_{-c/2}^{c/2}\delta p^{s}_{gh,\zeta j} \qquad \text{(A4.2)}$$

Substituting Eq. (A4.1) into Eq. (A4.2) and using identities (A2.3) and (A2.5), we obtain the nth component of sound pressure as

$$p^{s}_{gh,n} = \int_{r_h}^{r_t}\hat{U}_{gh,r}\frac{-i\rho_o a_o K_{mgh}}{4\pi R}(-i)^m \exp\{-iK_{mgh}\, a_o(t - R/a_o) + i\phi_{gh}\}$$

$$X\quad B\cdot G_{mgh}\cdot J_m(K_{mgh}\, r\sin\Psi)\cdot dr \qquad \text{(A4.3)}$$

where $K_{mgh} = (\omega_h - g\Omega + m\Omega)/a_o$

$m = nB + g,$

and

$$G_{mgh} = \int_{-c/2}^{c/2} \frac{db}{d\zeta} \cdot \exp\{im(\zeta \sin\lambda)/r + iK_{mgh}(\zeta \cos\lambda)\cos\Psi\} \cdot d\zeta \qquad \text{(A4.4)}$$

We note that tone noise at blade passing frequency exists only when $\omega_h = 0$, i.e. for steady state inflow distortion. Using the value at representative radius r_e, for the integrand in Eq. (A4.3), we can write the following expression for the rms value of the nth harmonic of acoustic pressure due to gth component of steady state inflow distortion.

$$\tilde{p}^{s}_{gn} = \frac{\rho_o \, nB\Omega}{4\sqrt{2}\pi R} \cdot \hat{U}_{gr} \cdot B \cdot G_{mge} \cdot J_m(K_{nB} \, r_e \sin\Psi) \cdot (r_t - r_h) \qquad \text{(A4.5)}$$

where $K_{nB} = nB\Omega/a_o$

$m = nB + g,$

and

$$G_{mge} = \int_{-c/2}^{c/2} \frac{db}{d\zeta} \exp\{im(\zeta \sin\lambda)/r + iK_{nB}(\zeta \cos\lambda)\cos\Psi\} \cdot d\zeta \qquad \text{(A4.6)}$$

evaluated at $r = r_e$

We note that the far field sound pressure given by Eq. (A4.5) depends upon evaluating the integral of Eq. (A4.6) for the specific blade section profile, at each value of azimuth angle and the particular values of the indicies n and g. To illustrate the evaluation of the function G_{mge}, let us consider the double circular arc profile described by

$$\frac{db}{d\zeta} = -4(\zeta/c_e)(b/c)_{max,e} \qquad \text{(A4.7)}$$

where c_e is the blade chord and $(b/c)_{max,e}$ is the thickness

ratio of the blade section, both considered at the representative radius r_e. Using Eq. (A4.7) and the following notations

$$\frac{\zeta}{c/2} = \eta,$$

and
$$\mu = m(\tfrac{c}{2}\sin\lambda)/r_e + K_{nB}(\tfrac{c}{2}\cos\lambda)\cos\Psi \qquad \text{(A4.8)}$$

we can rewrite Eq. (A4.6) as

$$G_{mge} = -b_{max,e}\int_{-1}^{1} \eta \cdot e^{i\mu\eta}\, d\eta \qquad \text{(A4.9)}$$

From the value of the above definite integral we can show that

$$|G_{mge}| = 2b_{max,e}\left|\frac{\cos\mu}{\mu} - \frac{\sin\mu}{\mu^2}\right| \qquad \text{(A4.10)}$$

where μ is defined by Eq. (A4.8).

In evaluating sound pressure at blade passing frequency at on-axis points on the small scale fan, we note that

$$\mu = .28$$

leading to

$$|G_{mge}| = .1656\ b_{max,e} \qquad \text{(A4.11)}$$

A5 Monopole Radiation from Random Sources

Substituting Eq. (4.11) into Eq. (4.12) and using Eq. (A1.2) for the far field approximations, we obtain

$$\delta p^{s}_{\zeta j} = \frac{\rho_o}{2\pi} \sum_m \sum_g A_g \int_{\omega=-\infty}^{\infty} \frac{-iK_{mg}a_o}{4\pi R}$$

$$\times \exp\{-iK_{mg}a_o(t - R/a_o) - ig\theta_o\}$$

$$\times \exp\{im\theta - iK_{mg}\, r \sin\Psi \cos\theta\}$$

$$\times \exp\{im\zeta \sin\lambda/r + iK_{mg}\zeta \cos\lambda \cos\Psi\}$$

$$\times \exp\{-i(m - g)(j - 1)2\pi/B\} \cdot \frac{db}{d\zeta} \cdot d\zeta\, dr\, d\theta \cdot dZ_{u_r}(\omega) \qquad \text{(A5.1)}$$

where $K_{mg} = (\omega - g\Omega + m\Omega)/a_o$.

Following the procedure employed in the previous subsection A 3 step by step, we can easily derive the following expression for spectral density of far field acoustic pressure due to blade thickness effect

$$\Phi^{s}(\nu) = \frac{1}{2} \int_{r_h}^{r_t} (\nu\rho_o/4\pi R)^2 \ell_2(2\pi r/\ell_3)\, B^2$$

$$\times \sum_m \sum_g A_m^2 |G_{mge}|^2 \Phi_{u_r}(\omega) \cdot J_m^2\left(\frac{\nu}{a_o} r \sin\Psi\right) dr \qquad \text{(A5.2)}$$

where $m = nB + g$

$$\omega = \nu - m\Omega + g\Omega$$

and

$$G_{mge} = \int_{-c/2}^{c/2} \frac{db}{d\zeta} \exp\{im(\zeta \sin\lambda)/r + i\frac{\nu}{a_o}(\zeta \cos\lambda)\cos\Psi\} \cdot d\zeta \qquad \text{(A5.3)}$$

evaluated at $r = r_e$

We note that Eq. (A5.3) is similar to Eq. (A4.6). Thus the amplitude of G_{mge} in Eq. (A5.2) can be evaluated from Eq. (A4.10) and Eq. (A4.8) with K_{nB} replaced by ν/a_o.

A6 RADIATION FROM ORDERED QUADRUPOLES

Confining our discussion to longitudinal axial quadrupoles only, the "fluctuating Reynolds stresses" due to the interaction of steady state inflow distortion and the potential velocity perturbation is given by Eq. (3.19). The far field acoustic pressure radiated by these "fluctuating Reynolds stresses" can be obtained by substituting Eq. (3.19) into Eq. (3.17) to give

$$\delta p_n^q = \frac{-2\rho_o K_{nB}}{4\pi R} \cos^2\Psi \, \hat{U}_{g,1} \, \hat{U}_{p_1,n} \exp\{-2\pi\eta_1 |n|/d\}$$
$$\times \exp\{-iK_{nB} a_o (t - R/a_o)\}$$
$$\times \exp\{im\theta - iK_{nB} r \sin\Psi \cos\theta\}$$
$$\times \exp\{i\phi_{p_1,n} - iK_{nB} \eta_1 \cos\Psi\} r dr \, d\theta \, d\eta_1 \qquad \text{(A6.1)}$$

where $m = nB + g$

and $K_{nB} = nB\Omega/a_o$.

To include the radiation from all the quadrupoles present in the region upstream of the rotor, we can integrate Eq. (A6.1) over the region

$$0 < \eta_1 < \infty$$
$$0 \leq \theta \leq 2\pi$$
$$r_h \leq r \leq r_t$$

to arrive at the following expression for the nth harmonic of the far field sound pressure due to the gth component of the inflow distortion,

$$p^q_{g,n} = \frac{2\rho_o K_{nB}}{4\pi R}\cos^2\Psi \int_{r_h}^{r_t} (-i)^m \hat{U}_{g,1}\ \hat{U}_{p_1,n}\ (d/n)$$

$$X\ \exp\{-iK_{nB}a_o(t - R/a_o) + i\phi_{p_1,n}\}$$

$$X\ J_m(K_{nB}\, r \sin\Psi) r \cdot dr \qquad \text{(A6.2)}$$

We have ignored the retarded time in the axial direction when performing the integration with respect to η_1 because the potential velocity perturbation decay very fast in the axial direction.

Using a representative radius r_e and replacing the integrand of the above Eq. (A6.2) by its value at r_e, we can write the rms value of the nth harmonic as

$$\tilde{p}^q_{g,n} = \frac{\rho_o K_{nB}}{4\sqrt{2}\pi R}\cos^2\Psi \cdot \frac{d_e}{|n|} \cdot 2\hat{U}_{g,1}\ \hat{U}_{p_1,n} \cdot J_m(K_{nB}\, r \sin\Psi) \cdot r_e (r_t - r_h) \qquad \text{(A6.3)}$$

where $m = nB + g$

and $K_{nB} = nB\Omega/a_o$.

A7 RADIATION FROM RANDOM QUADRUPOLE SOURCES

Retaining only the product term $2U_{p_1} u_1$ in V_1^2, we note that Eq. (4.16) reduces to

$$R_{V_1^2}(\underset{\sim}{\eta}, \underset{\sim}{\xi}, \tau) = 4R_{U_{p_1} u_1}(\underset{\sim}{\eta}, \underset{\sim}{\xi}, \tau) \qquad \text{(A7.1)}$$

Since the periodic fluctuations U_{p_1} are not related to the inflow turbulence fluctuations u_1, the above space-time correlation function can be written as

$$R_{U_{p_1} u_1} = R_{U_{p_1}} \cdot R_{u_1} \tag{A7.2}$$

From the description of the nth component of U_{p_1} given in Eq. (2.5) we obtain

$$R_{U_{p_1,n}} = \frac{1}{2}\{\hat{U}_{p_1,n}\}^2 \cos(k_p \xi_3 - \omega_p \tau) \cdot \exp\{-2k_p \eta_1 - k_p \xi_1\} \tag{A7.3}$$

where $k_p = 2\pi n/d$

and $\omega_p = nB\Omega$

Substituting the above Eq. (A7.3), Eq. (2.9) and Eq. (A7.2) into Eq. (A7.1), the required space-time correlation function can be written as

$$R_{V_1^2}(\underset{\sim}{\eta}, \underset{\sim}{\xi}, \tau) = 2\{\hat{U}_{p_1,n}\}^2 \cdot \overline{u^2} \cdot \cos(k_p \xi_3 - \omega_p \tau)$$
$$\exp\left\{-2k_p \eta_1 - k_p \xi_3 - |\xi_1 - U_a \tau|/\ell_1\right.$$
$$\left. - |\xi_2|/\ell_2 - |\xi_3|/\ell_3\right\} \tag{A7.4}$$

The above equation is then substituted into Eq. (4.15) and integration over the flow region is performed to obtain Eq. (4.17). In carrying out the integration the retarded time difference τ^* is ignored since the fluctuations $U_{p_1,n}$ decay rapidly with η_1. The integration being only over the upstream region of the rotor, the ranges of $\underset{\sim}{\eta}$ and $\underset{\sim}{\xi}$ are restricted by the following limits

$$-\eta_1 \leq \xi_1 \leq \infty \qquad \text{and} \qquad 0 \leq \eta_1 \leq \infty$$

REFERENCES

1. Rao, G.V.R. and Associates, "Study of Non-radial Stators for Noise Reduction", NASA CR-1882, September, 1971.

2. Kazin, S.B. and Volk, L.J., "LF336 Lift Fan Modification and Acoustic Test Program", NASA CR-1934, December, 1971.

3. Rao, G.V.R., et al, "Analytical Lift Fan Noise Study", NASA CR-114576, July 13, 1972.

4. Lighthill, M.J., "Sound Generated Aerodynamically" The Bakerian Lecture, Proc. Roy. Soc. (London), Vol. 276, Series A, 1962, pp 147-186.

5. Hanson, D.B., "A Unified Analysis of Fan Stator Noise", presented at 84th meeting of Acous. Soc. Am., Miami Beach, Fla., Nov. 28 - Dec. 1, 1972

6. Deming, A.F., "Noise from Propellers with Symmetrical Sections at Zero Blade Angle, II", NACA TN 679, 1938.

7. Lighthill, M.J., "On Sound Generated Aerodynamically", Proc. Roy. Soc. (London), A211, 1952, pp 564-687.

8. Kemp, N.H. and Sears, W.R., "The Unsteady Forces Due to Viscous Wakes in Turbomachines", J. Aerospace Sci., Vol. 19, 1952, pp 713.

9. Gutin, L., "On the Sound Field of a Rotating Propeller", NACA TM 1195, 1948 (Physikalische Zeitschrift der Sowjetunion, Band 9, Heft 1, 1936, pp 57-71).

10. Sveshnikov, A.A., Applied Methods of the Theory of Random Functions, Pergamon Press, New York, 1966.

11. Rao, G.V.R. et al, "Rotor Noise Due to Inflow Turbulence", A.I.A.A. paper No. 73-632, 6th Fluid and Plasma Dynamics Conference, Palm Springs, Calif. July 1973.

12. Mani, R., "Noise Due to Interaction of Inlet Turbulence with Isolated Stators and Rotors", J. Sound Vib., Vol. 17, No. 2, 1971, pp 123-132.

13. Homicz, G.F. and George, A.R., "Broadband Radiation from Rotors in Turbulent Flow", Proc. Interagency Symposium on Univ. Research in Transportation Noise, Stanford University, March 1973.

14. Chu, W.T., "Turbulence Measurements Relevant to Jet Noise", UTIA Rpt. 119, Nov. 1966.

15. Chandrashekhara, N., "Sound Radiation from Inflow Turbulence in Axial Flow Fans", J. Sound Vib., Vol. 19, No. 2, 1971.

16. Ffowcs Williams, J.E. and Hawkings, D.L., "Theory Relating to the Noise of Rotating Machinery", J. Sound Vib., Vol. 10, No. 10, 1969.

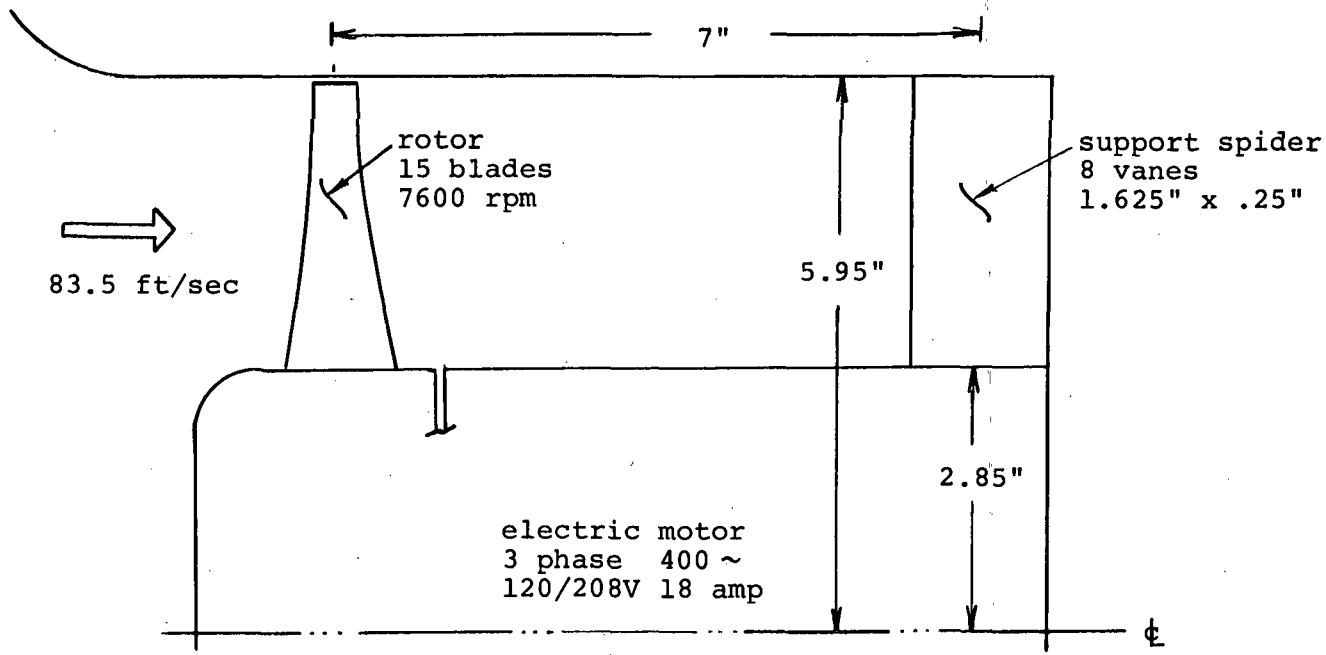

location	hub	pitch	tip
Blade chord	1.50in	1.40in	1.38in
Stagger angle	48^0	63^0	70^0

Fig. 1.1 Sketch of the Small Scale Fan and the Rotor Blade Parameters

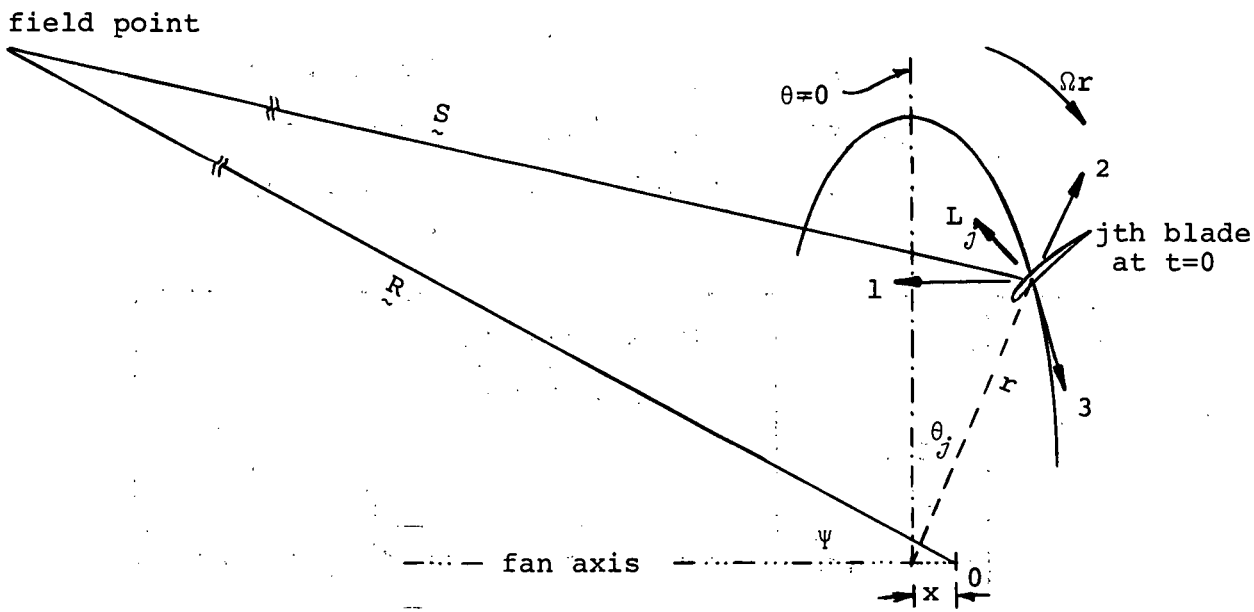

Fig. 2.1 Coordinate System and Location of a Blade

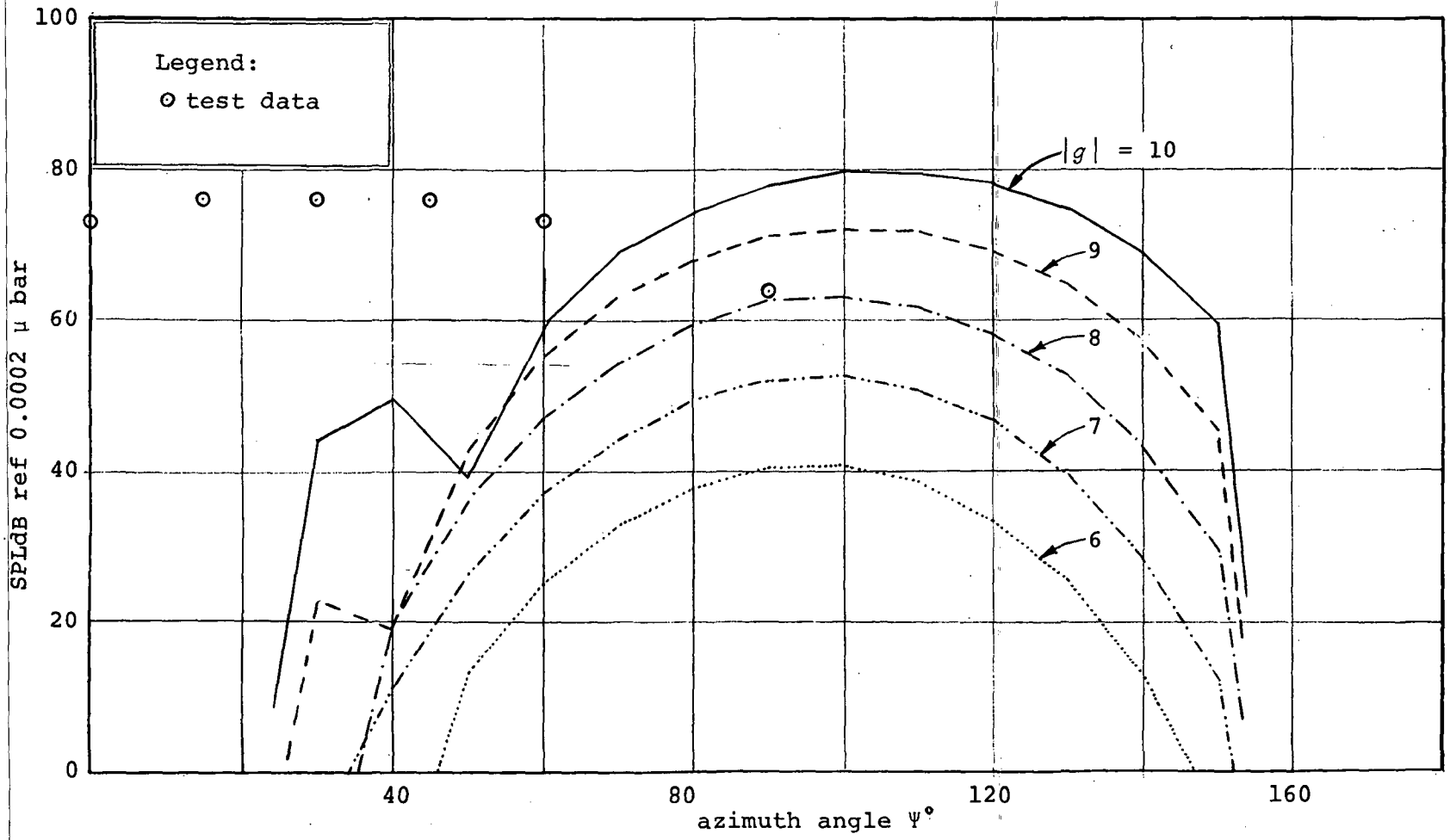

Fig. 3.1 Effect of gth Component of Inflow Distortion on Blade Passing Frequency Noise at 5 ft. from the Small Scale Rotor (computed from periodic blade loading)

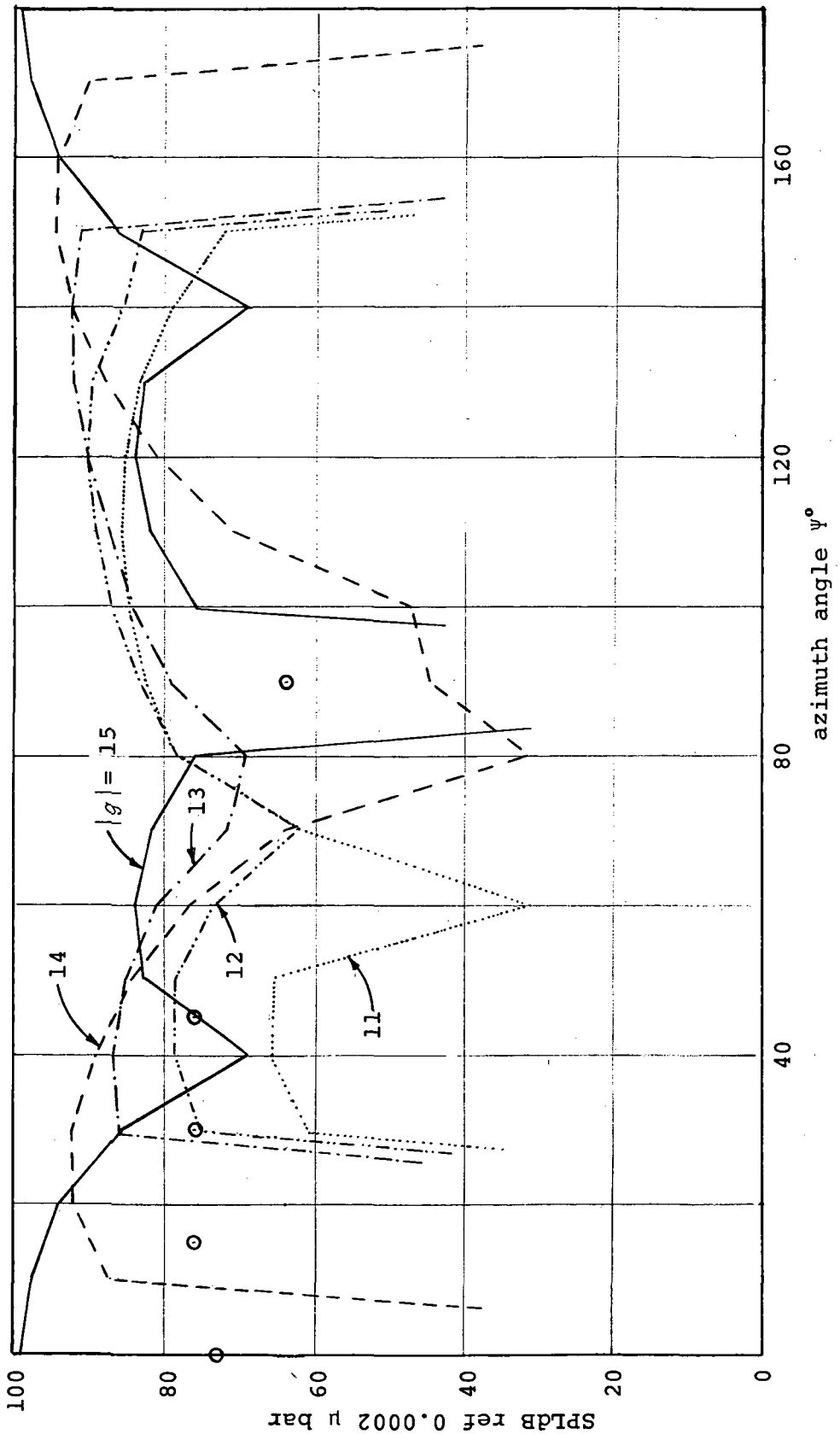

Fig. 3.1 continued

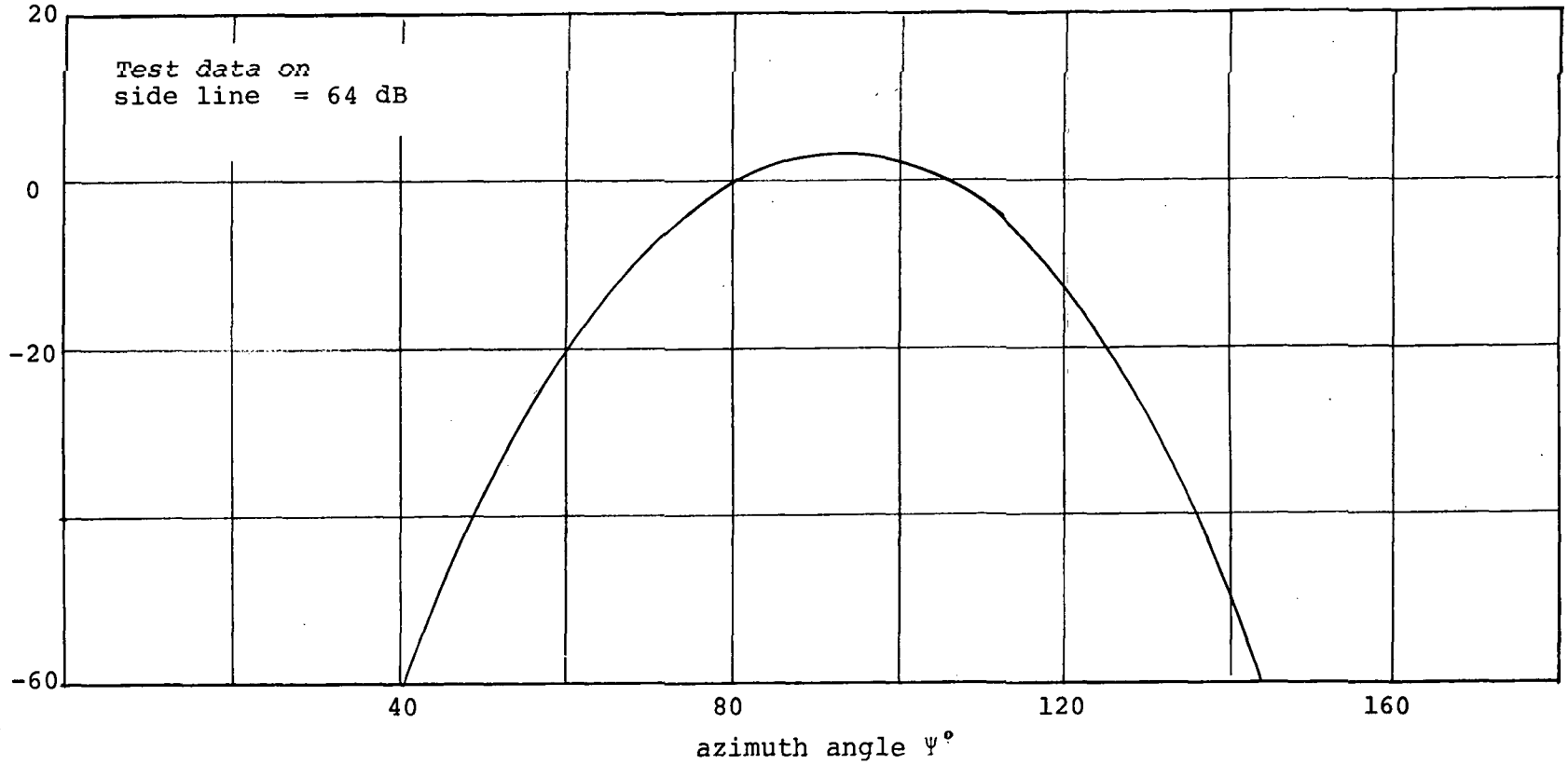

Fig. 3.2 Blade Passing Frequency Noise at 5 ft. from the Small Scale Rotor in Uniform Flow
(computed from steady state blade loading)

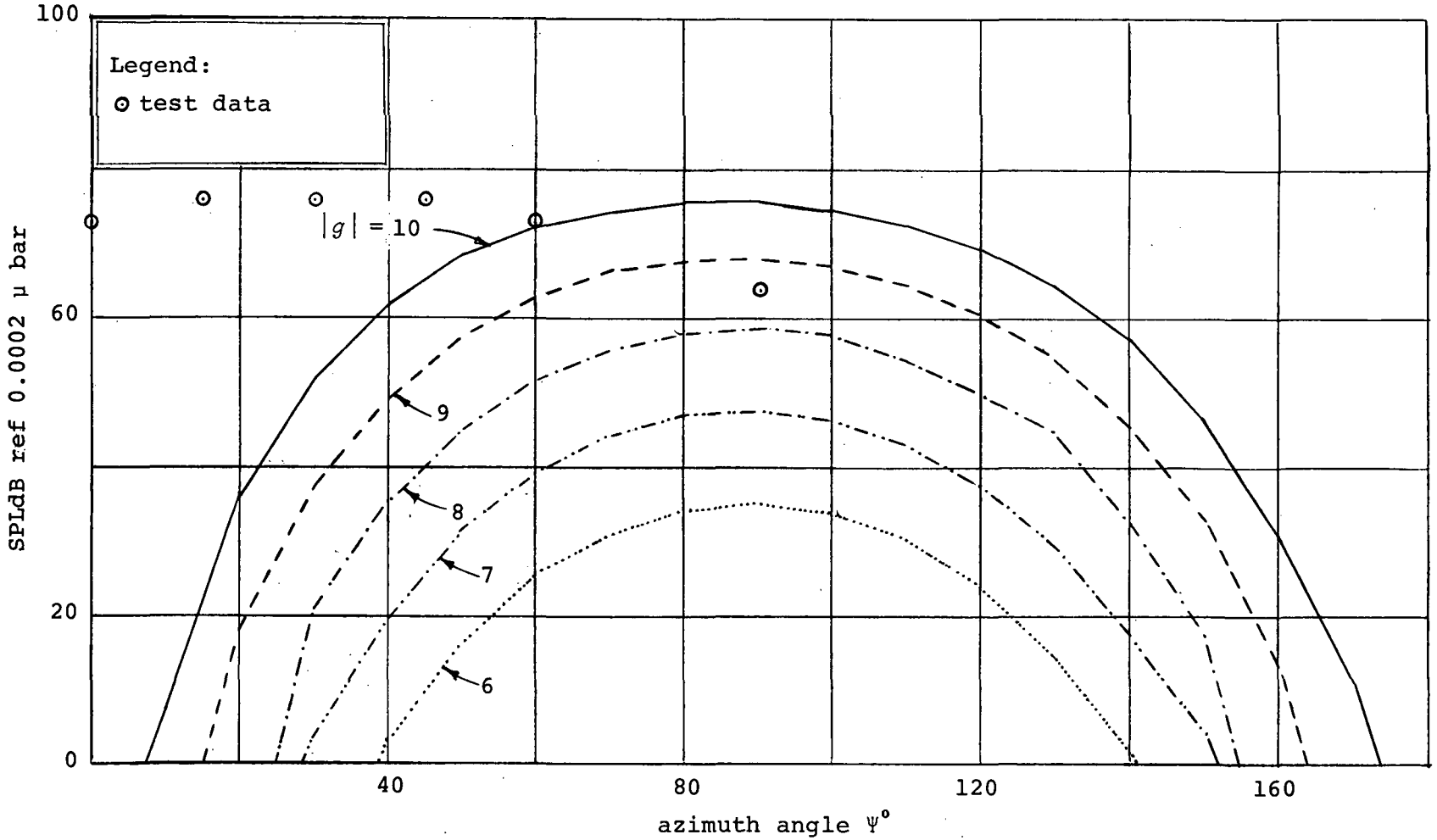

Fig. 3.3 Effect of gth Component of Inflow Distortion on Blade Passing Frequency Noise at 5 ft. from the Small Scale Rotor (computed from blade thickness effect)

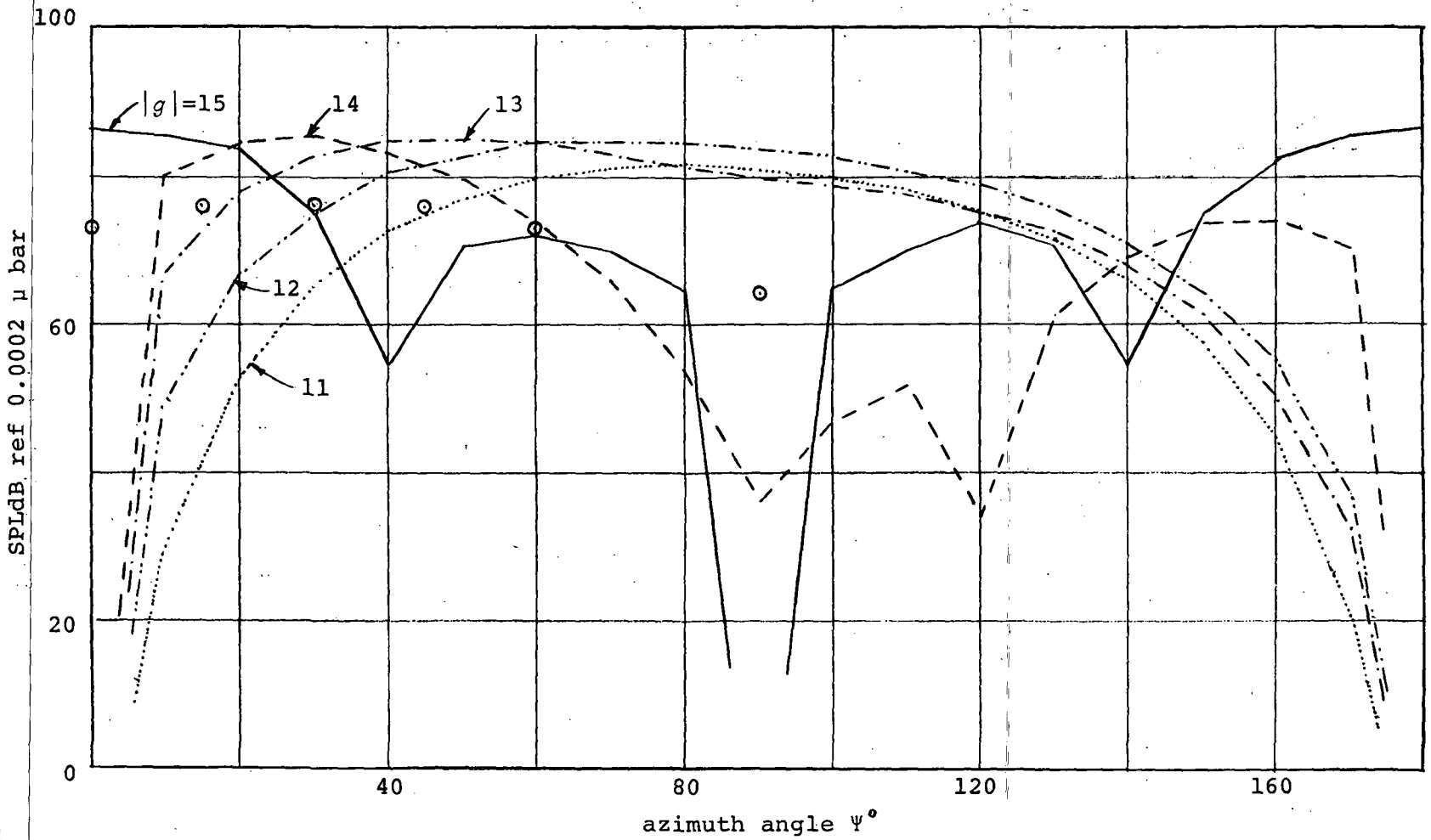

Fig. 3.3 continued

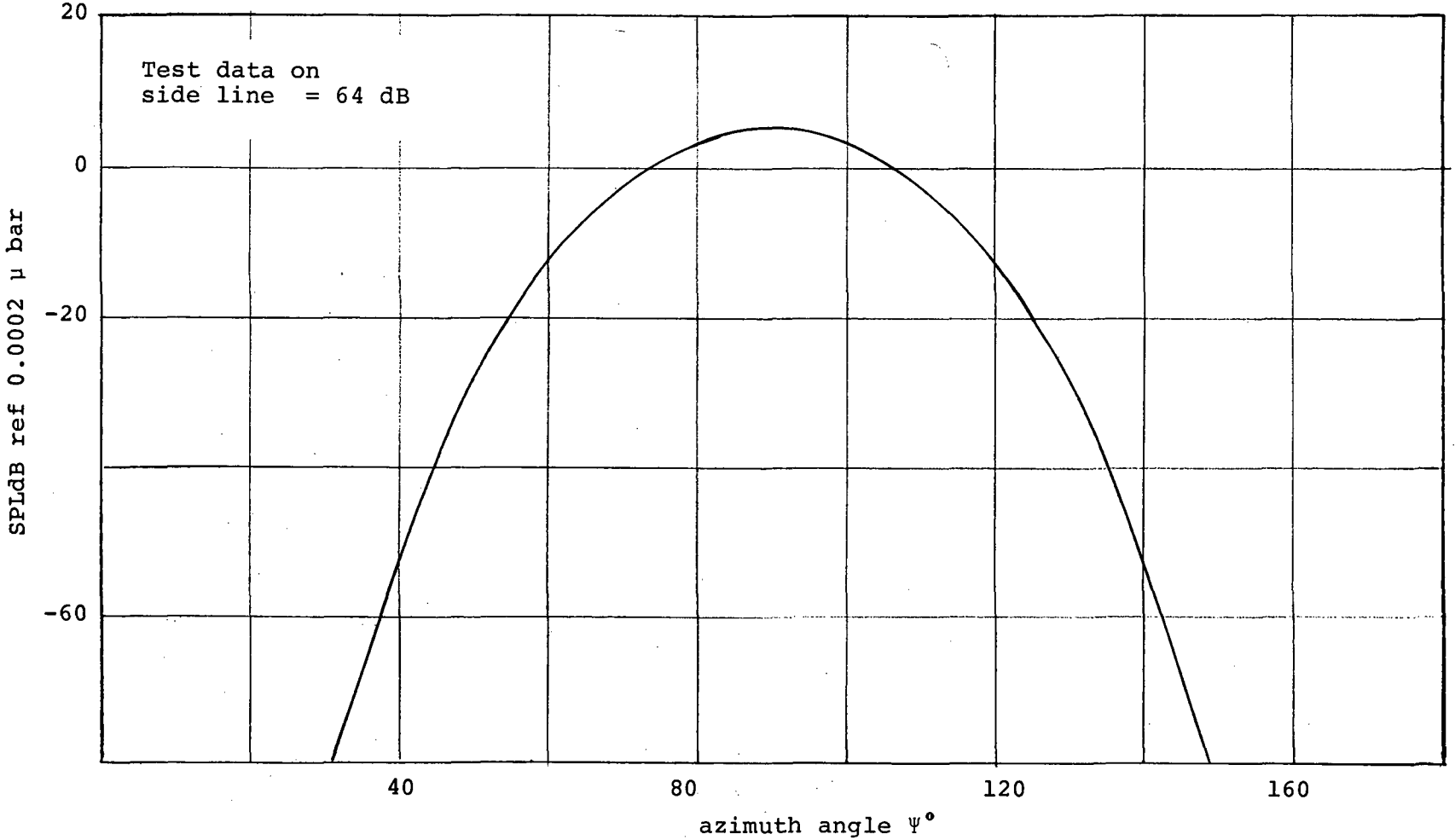

Fig. 3.4 Blade Passing Frequency Noise at 5 ft. from the Small Scale Rotor in Uniform Flow
(computed from blade thickness effect)

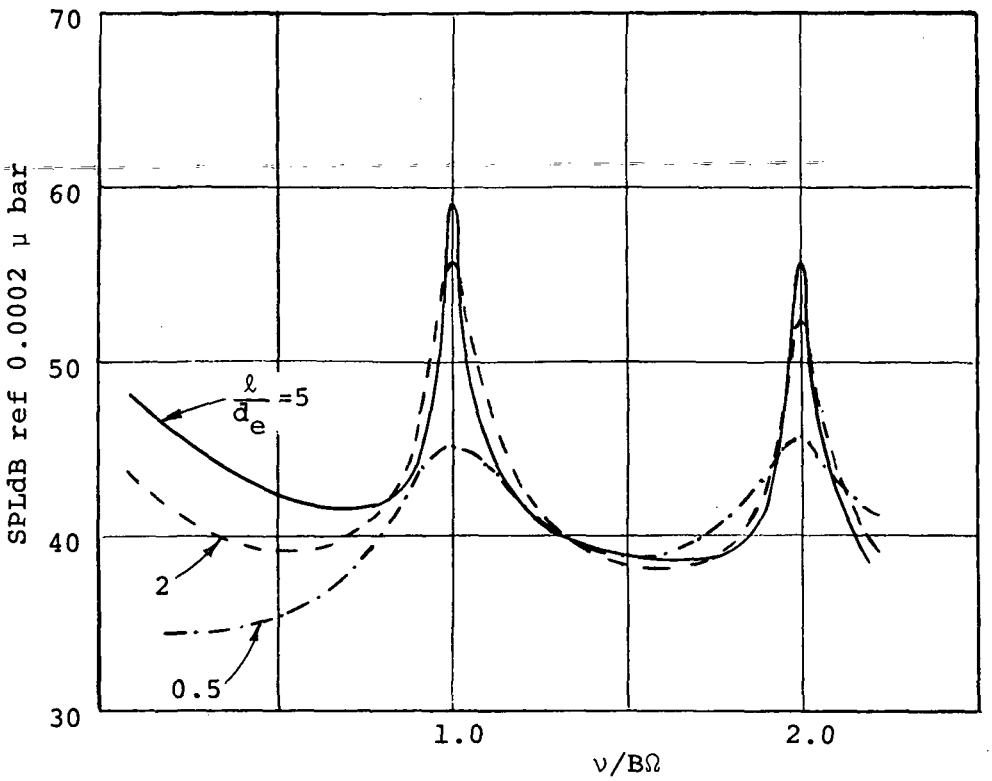

Fig. 4.1 Noise Spectrum at On-axis Point 5 ft. from Small Scale Rotor (computed from random blade loading; 3% turbulence intensity)

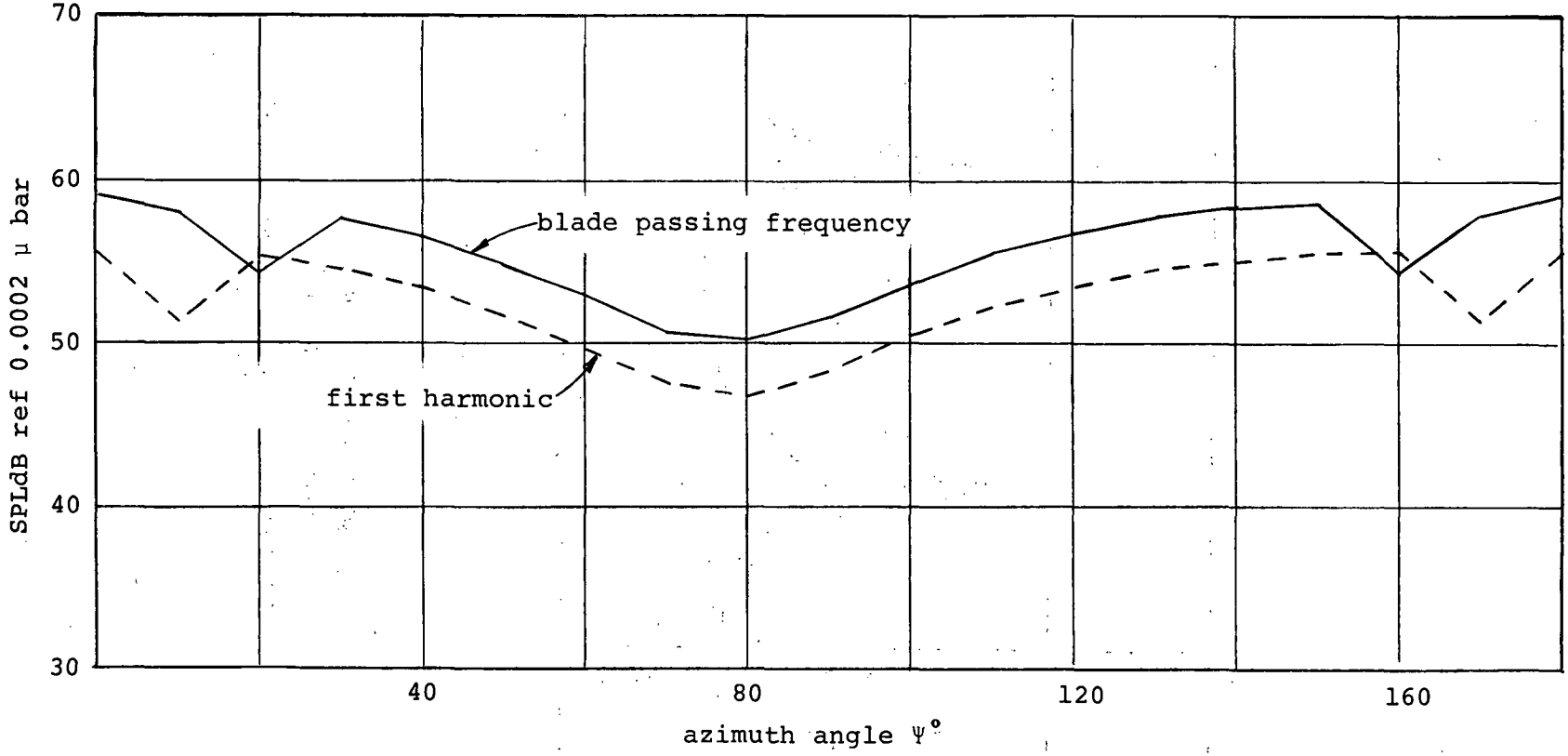

Fig. 4.2 Directivity of Discrete Tone Noise at 5 ft. from Small Scale Rotor (computed from random blade loading; 3% turbulence intensity)

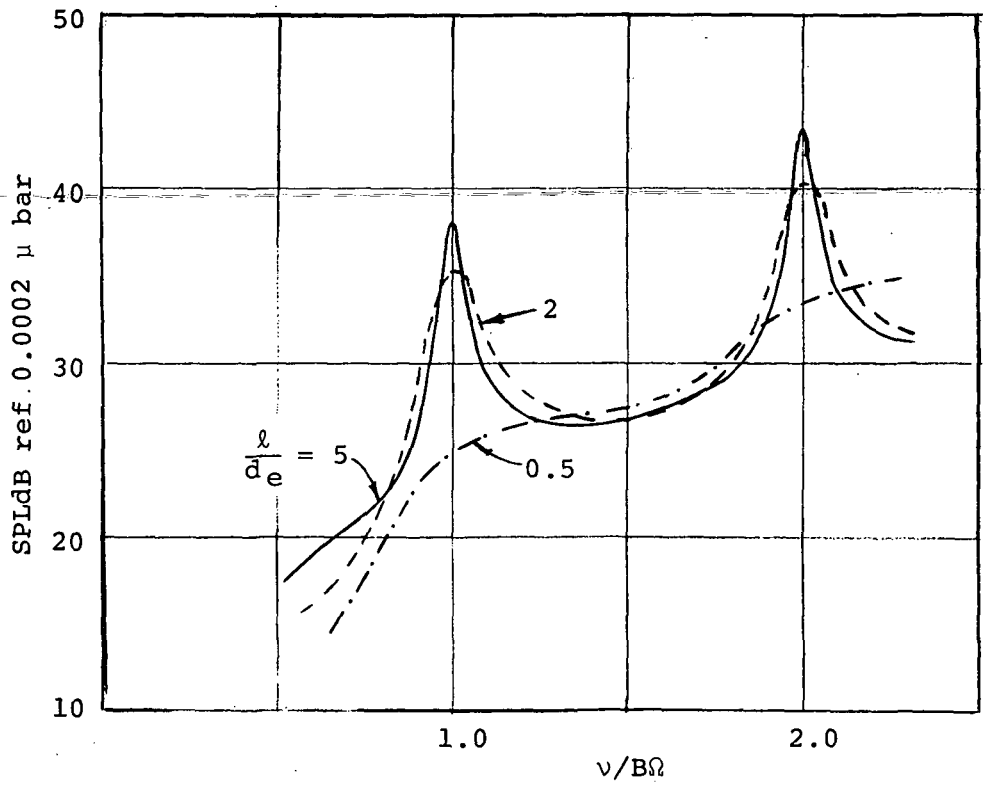

Fig. 4.3 Noise Spectrum at On-axis Point 5 ft. from Small Scale Rotor (computed from blade thickness effect; 3% turbulence intensity)

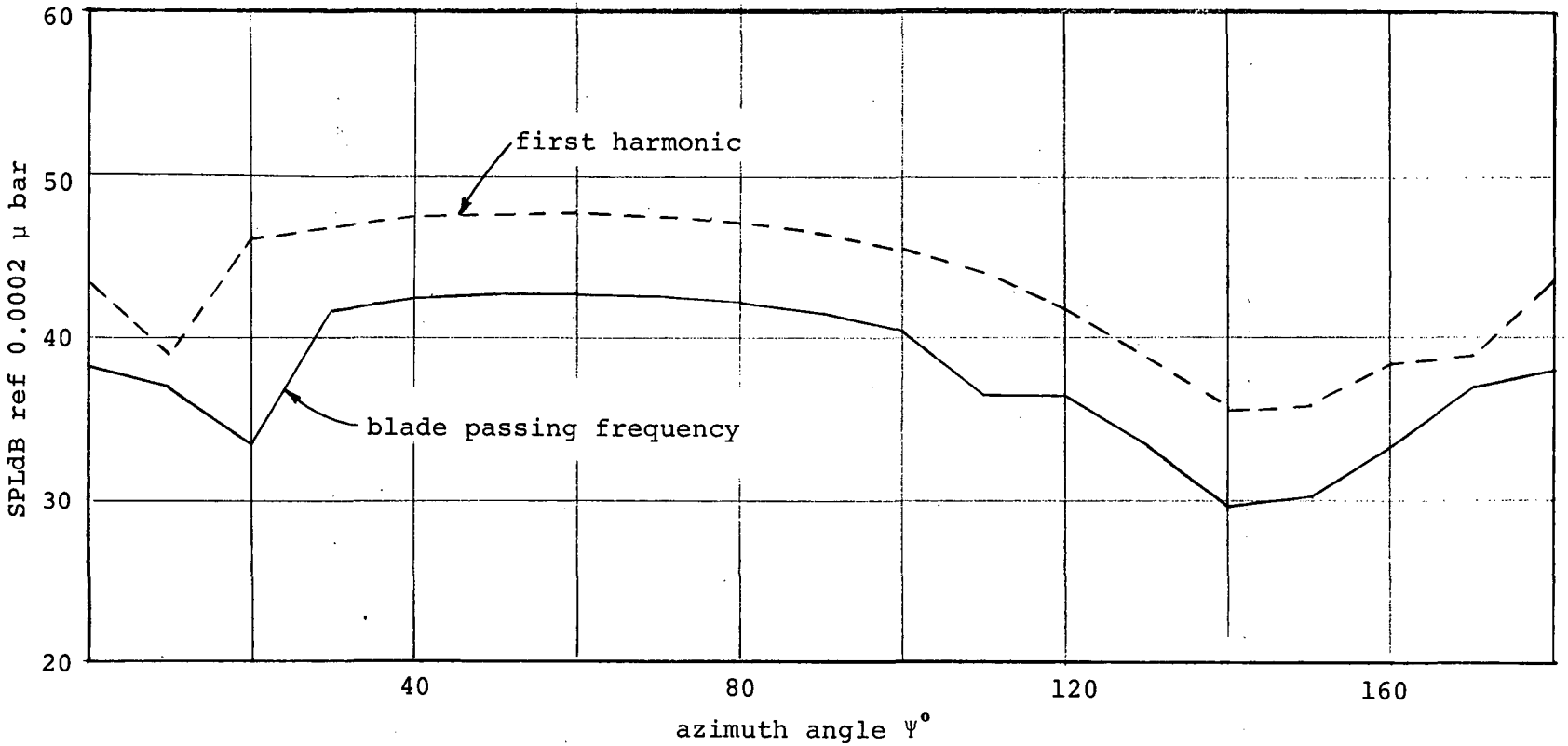

Fig. 4.4 Directivity of Discrete Tone Noise at 5 ft. from Small Scale Rotor (computed from blade thickness effect; 3% turbulence intensity)

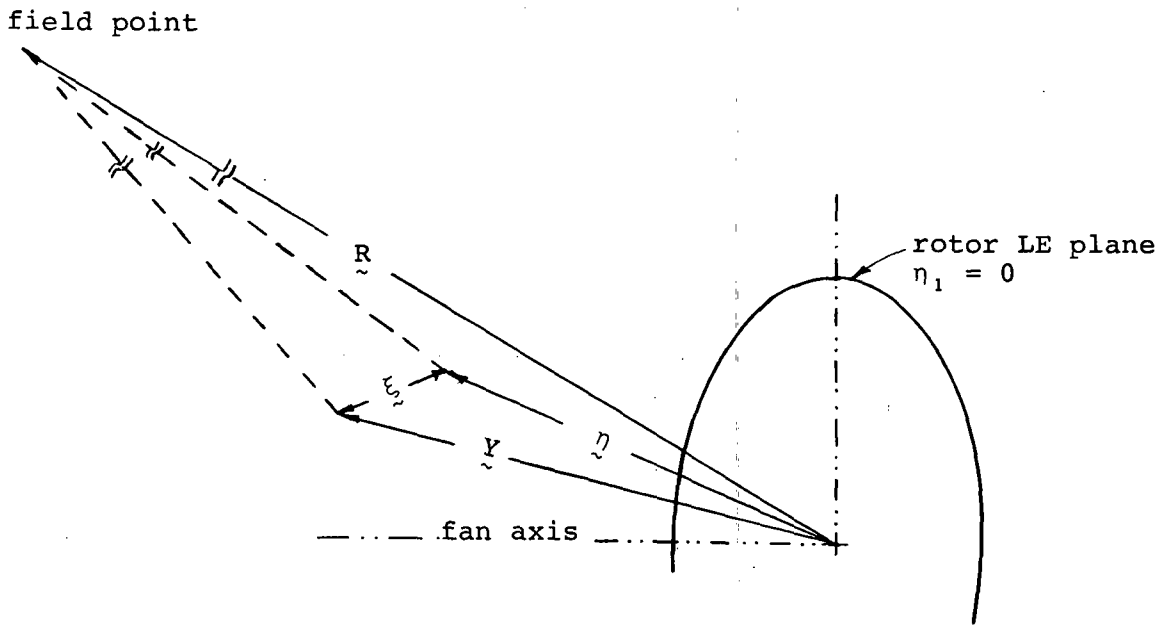

Fig. 4.5 Coordinate System Employed for Space-time Correlation Function of Velocity Functions

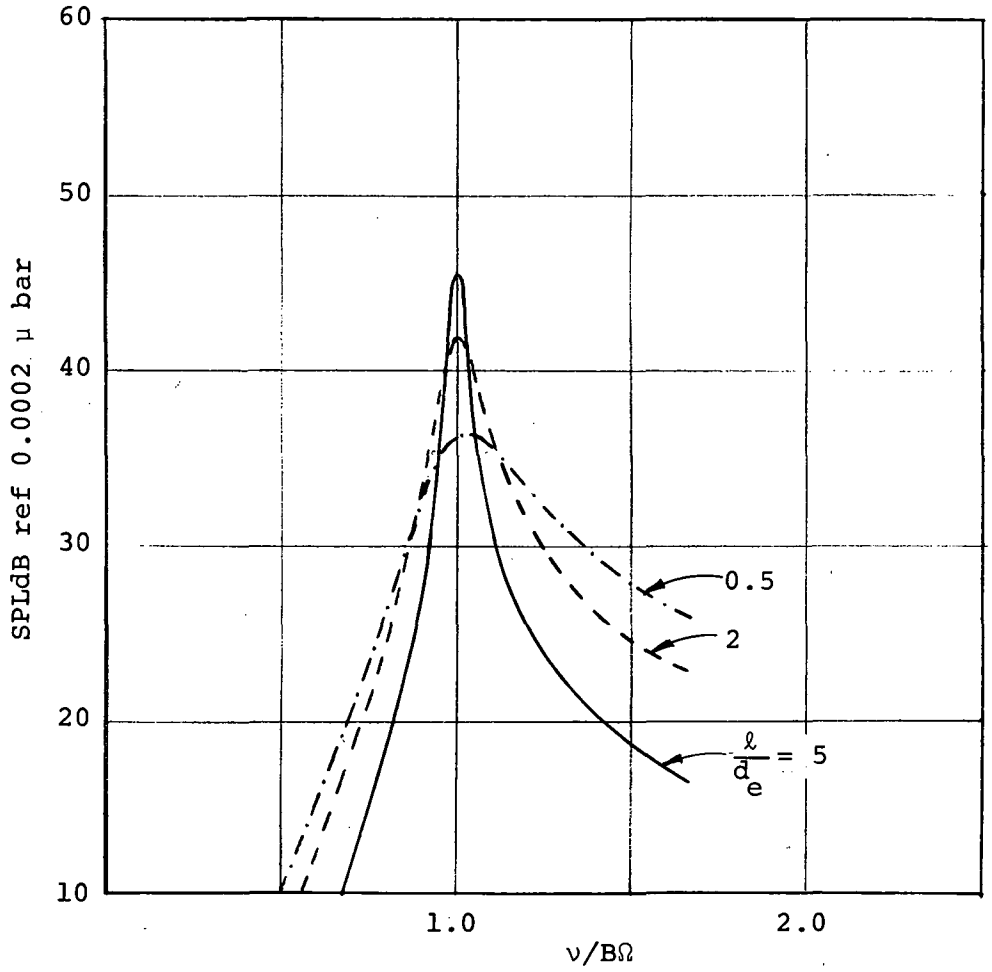

Fig. 4.6 Noise Spectrum at On-axis Point 5 ft. from Small Scale Rotor
(computed from longitudinal axial quadrupoles; 3% turbulence intensity)

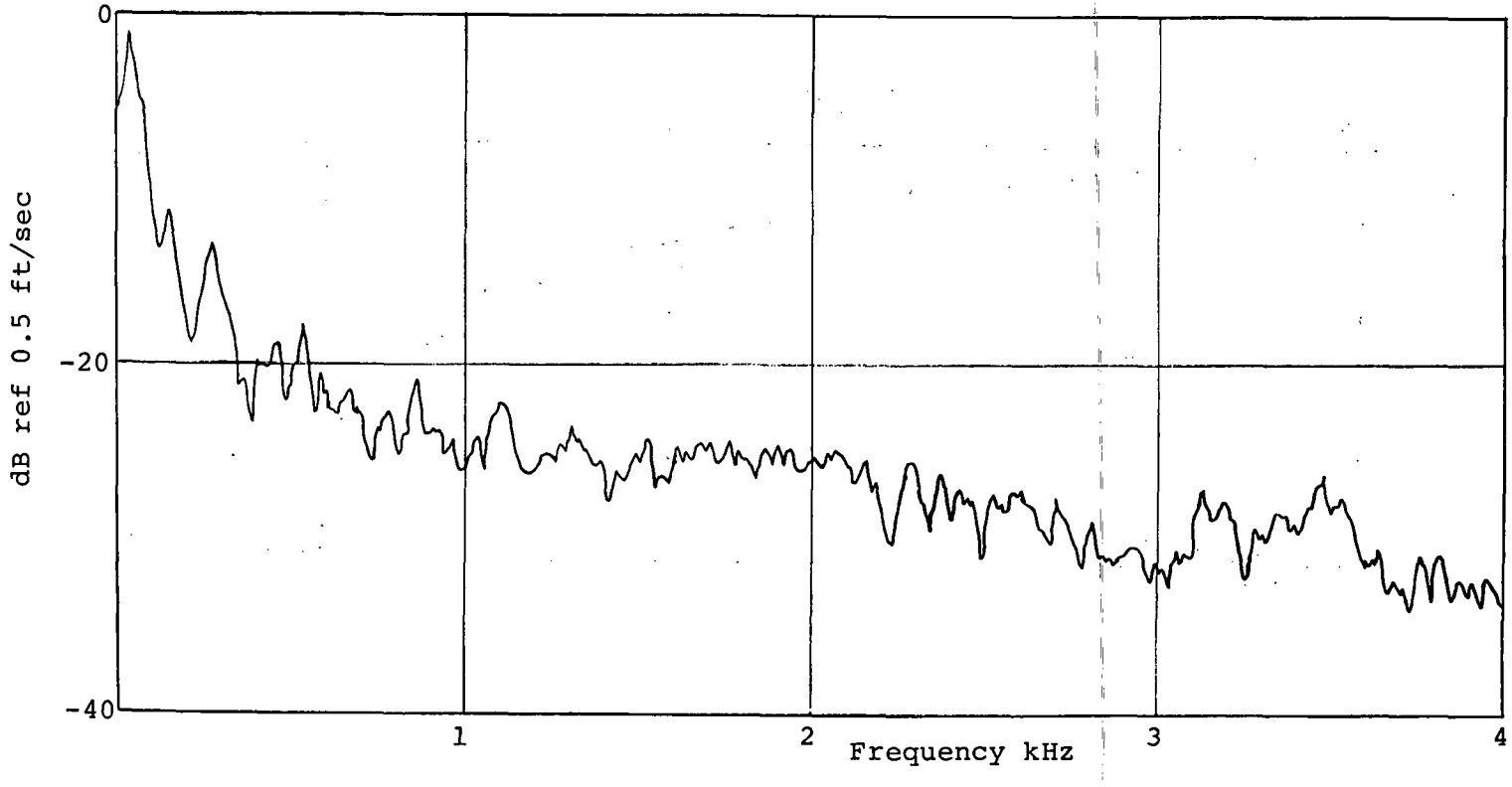

Fig. 5.1 Spectrum of the Axial Component of u from Test Data
(band width 50 Hz)

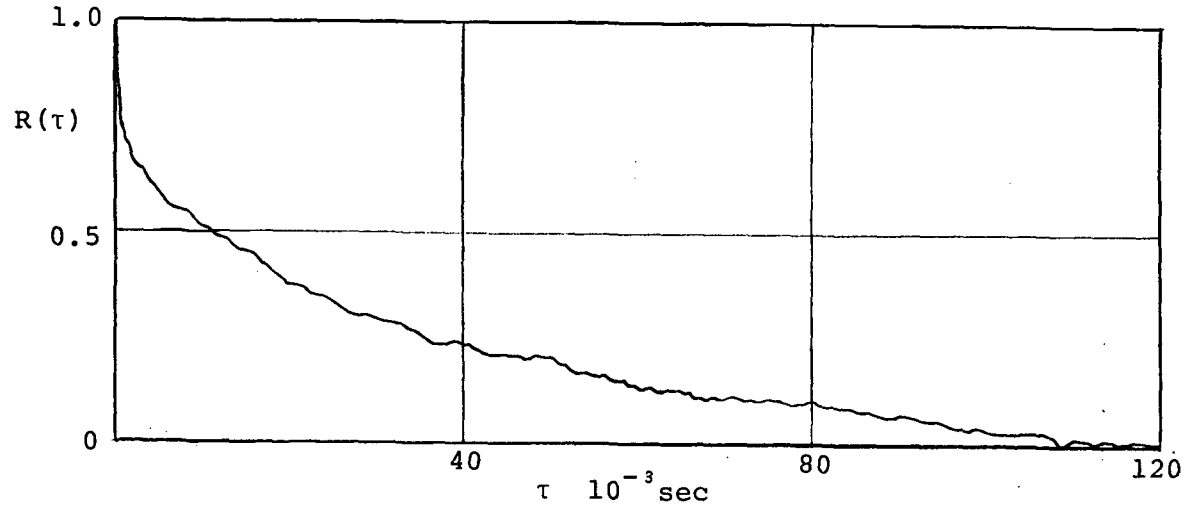

Fig. 5.2 Auto Correlation Function of the Axial Component of u from Test Data

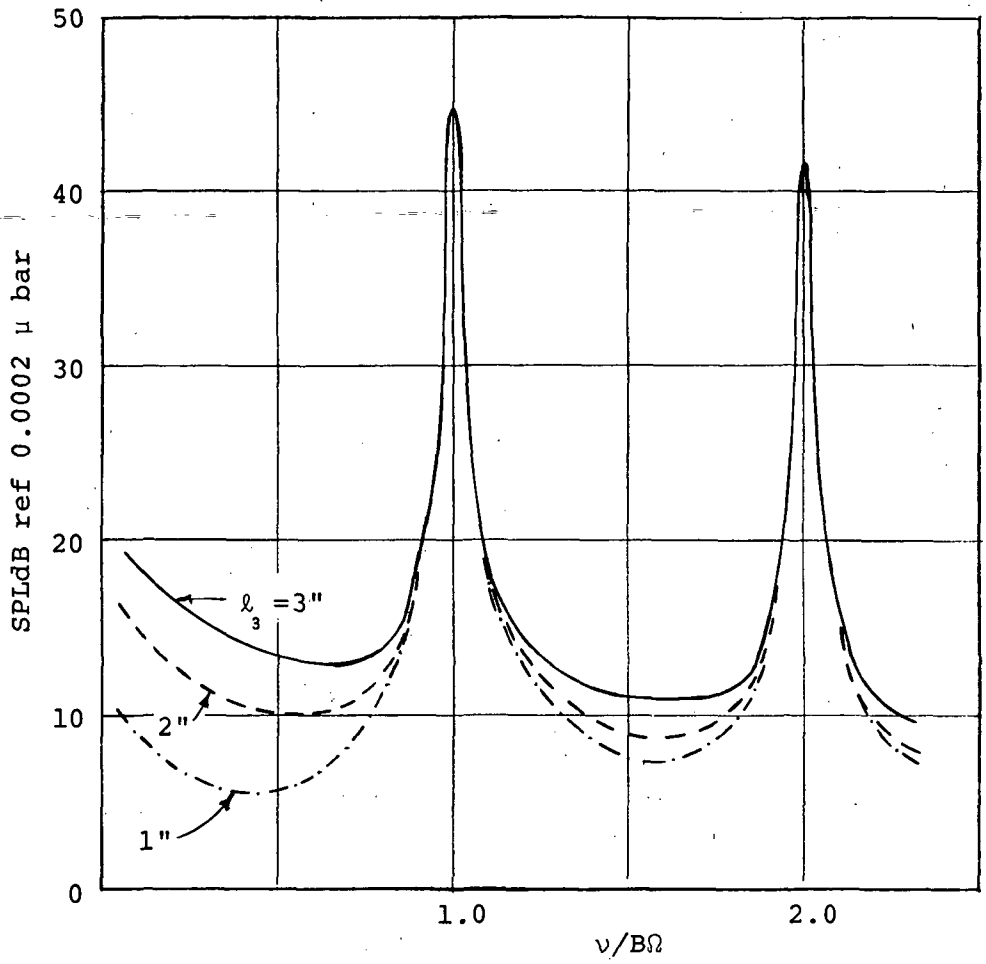

Fig. 5.3 Noise Spectrum at On-axis Point 7 ft. from Small Scale Rotor Computed from Blade Loading Corresponding to Measured Turbulence Parameters

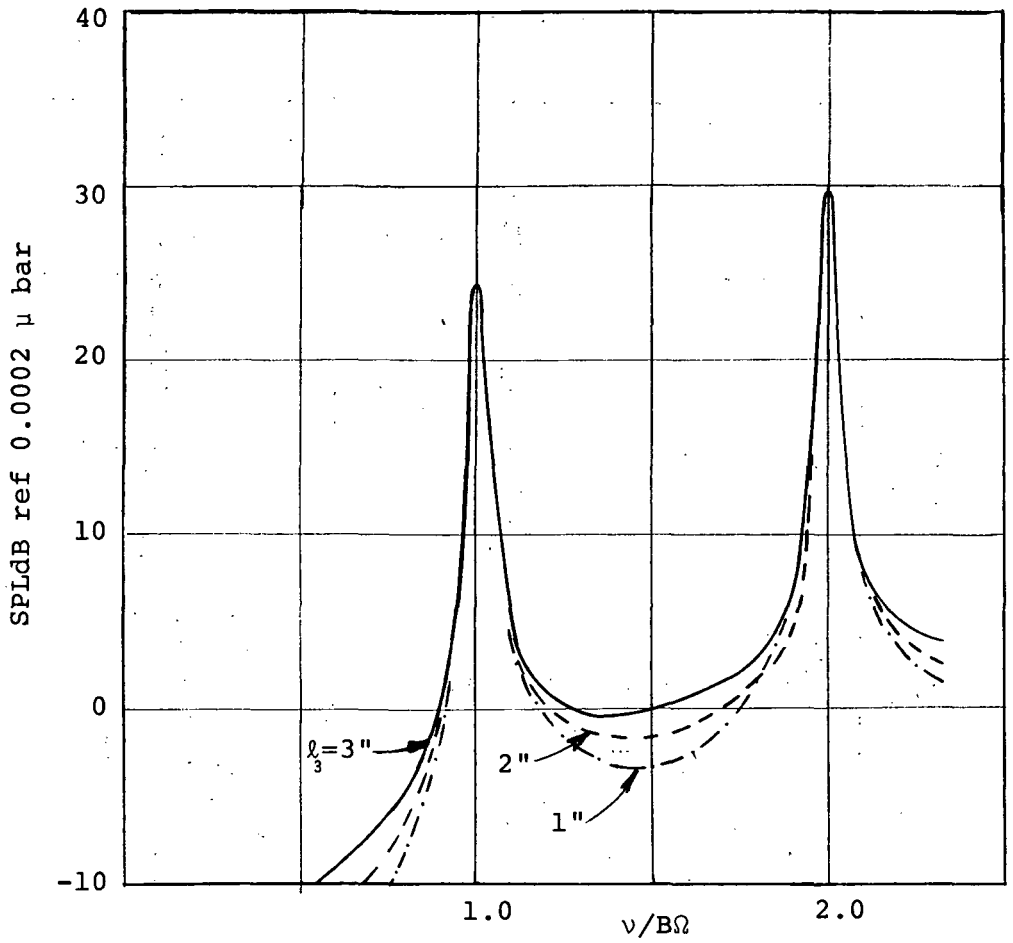

Fig. 5.4 Noise Spectrum at On-axis Point 7 ft. from Small Scale Fan Computed from Blade Thickness Effect Corresponding to Measured Turbulence Parameters

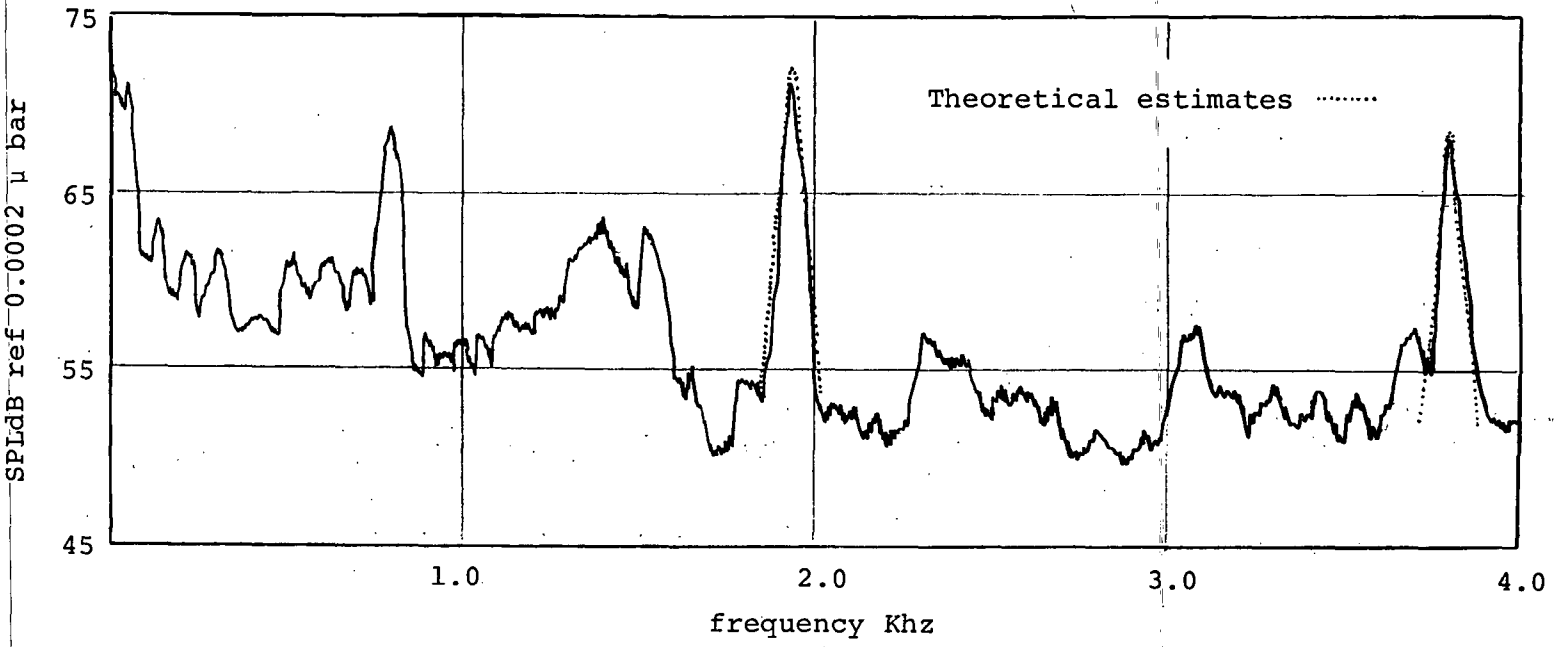

Fig. 5.5 Narrow Band Analysis of Noise Measured at the On-Axis Point (band width 50 Hz)

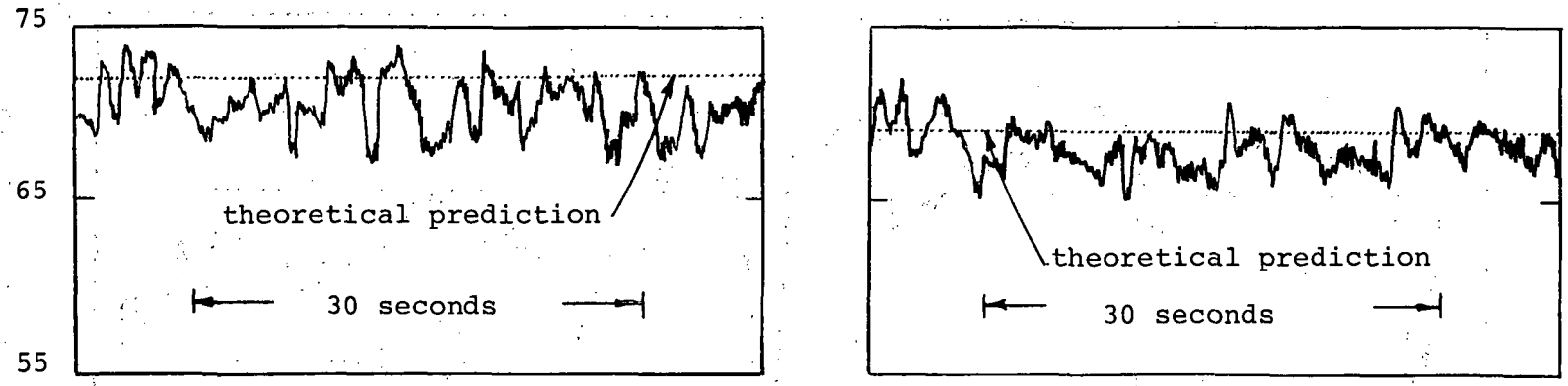

(a) blade passing frequency

(b) first harmonic

Fig. 5.6 Variability of Tone Levels Measured in the Tests
(50 Hz bandwidth centered at the tone)

NATIONAL AERONAUTICS AND SPACE ADMINISTRATION
WASHINGTON, D.C. 20546

OFFICIAL BUSINESS
PENALTY FOR PRIVATE USE $300

SPECIAL FOURTH-CLASS RATE
BOOK

POSTAGE AND FEES PAID
NATIONAL AERONAUTICS AND
SPACE ADMINISTRATION
451

U.S.MAIL

POSTMASTER: If Undeliverable (Section 158 Postal Manual) Do Not Return

"The aeronautical and space activities of the United States shall be conducted so as to contribute . . . to the expansion of human knowledge of phenomena in the atmosphere and space. The Administration shall provide for the widest practicable and appropriate dissemination of information concerning its activities and the results thereof."

—NATIONAL AERONAUTICS AND SPACE ACT OF 1958

NASA SCIENTIFIC AND TECHNICAL PUBLICATIONS

TECHNICAL REPORTS: Scientific and technical information considered important, complete, and a lasting contribution to existing knowledge.

TECHNICAL NOTES: Information less broad in scope but nevertheless of importance as a contribution to existing knowledge.

TECHNICAL MEMORANDUMS: Information receiving limited distribution because of preliminary data, security classification, or other reasons. Also includes conference proceedings with either limited or unlimited distribution.

CONTRACTOR REPORTS: Scientific and technical information generated under a NASA contract or grant and considered an important contribution to existing knowledge.

TECHNICAL TRANSLATIONS: Information published in a foreign language considered to merit NASA distribution in English.

SPECIAL PUBLICATIONS: Information derived from or of value to NASA activities. Publications include final reports of major projects, monographs, data compilations, handbooks, sourcebooks, and special bibliographies.

TECHNOLOGY UTILIZATION PUBLICATIONS: Information on technology used by NASA that may be of particular interest in commercial and other non-aerospace applications. Publications include Tech Briefs, Technology Utilization Reports and Technology Surveys.

Details on the availability of these publications may be obtained from:

SCIENTIFIC AND TECHNICAL INFORMATION OFFICE

NATIONAL AERONAUTICS AND SPACE ADMINISTRATION

Washington, D.C. 20546